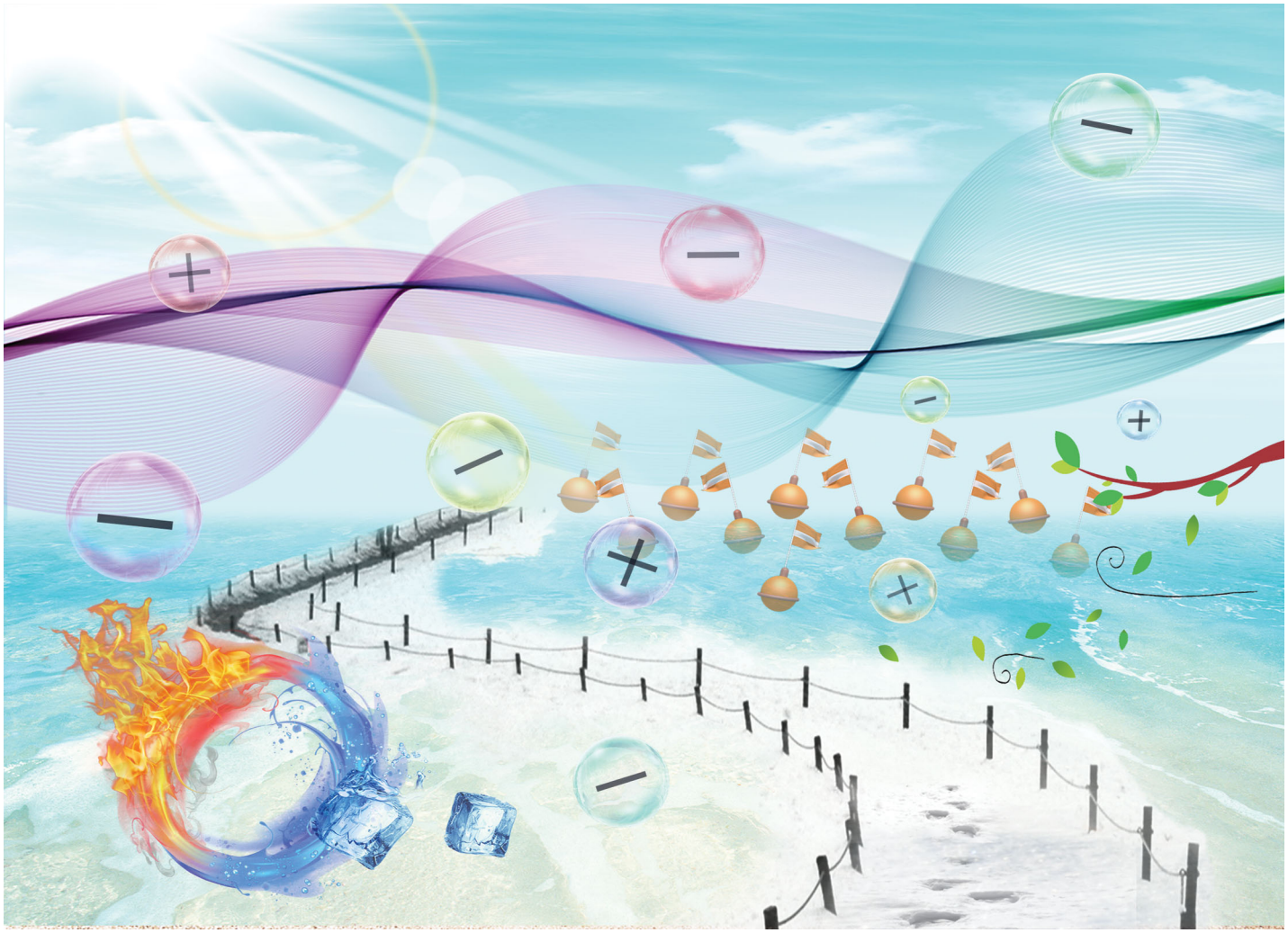

Featuring the work of Prof. Chris Bowen and co-workers: Dr Yan Zhang, Dr Mengying Xie, Dr Vana Adamaki and Dr Hamideh Khanbareh, University of Bath, UK.

Control of electro-chemical processes using energy harvesting materials and devices

Energy harvesting materials and devices can be coupled to electro-chemical systems, to provide new approaches for water splitting, catalysis, corrosion protection, degradation of pollutants, disinfection of bacteria and material synthesis.

As featured in:

See Mengying Xie *et al.*, *Chem. Soc. Rev.*, 2017, **46**, 7757.

ROYAL SOCIETY OF CHEMISTRY

rsc.li/chem-soc-rev

Registered charity number: 207890

Chem Soc Rev

REVIEW ARTICLE

View Article Online
View Journal | View Issue

Cite this: *Chem. Soc. Rev.*, 2017, **46**, 7757

Control of electro-chemical processes using energy harvesting materials and devices

Yan Zhang, † Mengying Xie,*† Vana Adamaki, Hamideh Khanbareh and Chris R. Bowen

Energy harvesting is a topic of intense interest that aims to convert ambient forms of energy such as mechanical motion, light and heat, which are otherwise wasted, into useful energy. In many cases the energy harvester or nanogenerator converts motion, heat or light into electrical energy, which is subsequently rectified and stored within capacitors for applications such as wireless and self-powered sensors or low-power electronics. This review covers the new and emerging area that aims to directly couple energy harvesting materials and devices with electro-chemical systems. The harvesting approaches to be covered include pyroelectric, piezoelectric, triboelectric, flexoelectric, thermoelectric and photovoltaic effects. These are used to influence a variety of electro-chemical systems such as applications related to water splitting, catalysis, corrosion protection, degradation of pollutants, disinfection of bacteria and material synthesis. Comparisons are made between the range harvesting approaches and the modes of operation are described. Future directions for the development of electro-chemical harvesting systems are highlighted and the potential for new applications and hybrid approaches are discussed.

Received 17th September 2017

DOI: 10.1039/c7cs00387k

rsc.li/chem-soc-rev

1. Introduction

Energy harvesting of heat, light and mechanical vibrations remains a vibrant topic. In many cases the harvester generates electrical energy, which is subsequently rectified, conditioned and stored within capacitors or batteries for applications such as wireless and self-powered sensors or low-power electronics. This review covers a new and emerging area that aims to directly couple energy harvesting materials and devices with electro-chemical systems.

There are excellent reviews available on electro-chemical storage materials[1,2] which focus on electro-chemical energy

Materials and Structures Centre, Department of Mechanical Engineering, University of Bath, BA1 7AY, UK. E-mail: M.Xie@bath.ac.uk
† These authors contributed equally to this work.

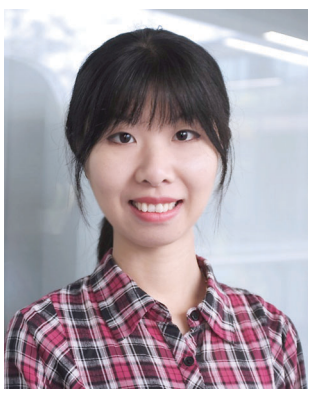

Yan Zhang

Yan Zhang obtained her BSc and PhD degrees in Materials Science from Central South University in 2008 and 2013, respectively. She worked in Hunan University from 2014 to 2016. Her PhD work concentrated on the fine adjustment of aligned porous structures and lead-free porous piezoelectric composite for biomedical application. She is currently a Marie-Skłodowska-Curie Fellow in Department of Mechanical Engineering in University of Bath, working on porous materials, ferroelectrics, bio-piezoelectric composite, sensors and energy harvesting applications since 2016.

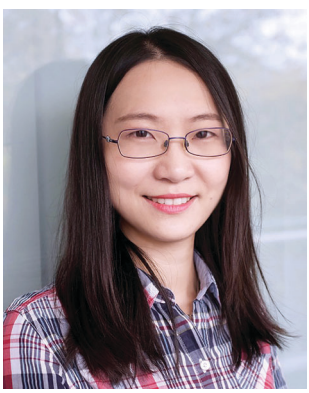

Mengying Xie

Mengying Xie has a BSc degree in Applied Physics from Tianjin University, China (2006–2010) and a PhD in Mechatronics Engineering from the University of Auckland, New Zealand (2010–2015). In 2016 she joined NEMESIS project in University of Bath as a postdoc. Her PhD work exploited the unique properties of PDMS into various wearable applications such as a flexible memory device, energy harvester from human motion and flexible force sensors. Her research area in Bath includes piezoelectric/pyroelectric energy harvesting for water splitting, piezoelectric sensors and smart energy storage applications.

storage configurations, such as flexible, fiber and transparent systems[1] and reviews which describe the potential of combining harvesting materials with conventional storage mechanisms to form self-powered electro-chemical energy storage systems (SEESs),[2] and multi-functional energy devices using super-capacitors and electro-chromic based systems.[3] Hybrid systems that to combine a variety of mechanical, thermal and light harvesting approaches have also been recently examined by Lee *et al.*[4]

This review will focus on exploitation of the harvested energy in electro-chemical applications. This will include water splitting, water treatment, catalysis, corrosion protection, degradation of pollutants, disinfection of bacteria and material synthesis. The intention of the review is not to overview the energy generation mechanisms, as these have been covered in detail elsewhere; for example see ref. 5–12. This review will provide a detailed overview of work to date on how energy harvesting materials and devices have been used to influence electro-chemistry; and aims to inspire new efforts in this emerging area. The coupling of energy generation with electro-chemistry is not entirely new and the intermittent nature of large scale renewable power generation methods, such as solar power[13] and wind energy,[14] has led to interest in using electrical energy to generate hydrogen from water which is then stored. Hybrid wind and light approaches are also under consideration.[15] However for smaller scale harvesting applications, typically in the μW to mW range, this is a more recent topic and has received significant recent attention for a diverse range of applications.

Harvesting approaches to be covered include pyroelectric,[5] piezoelectric,[6,7] triboelectric,[7,8] flexoelectric,[10] thermoelectric[9] and photovoltaic[12] effects, which are shown schematically in Fig. 1. The pyroelectric, piezoelectric and flexoelectric effects generate an electrical charge as a result of a change in polarisation of a material due to the application of a temperature change, applied stress or strain gradient respectively, while the photovoltaic effect arises from electrons being excited to the conduction band by solar energy. We will see in the review that these mechanisms of charge generation can take the form of an external bulk material or harvesting device that is connected to an electro-chemical cell, or it can take the form of electro-active particles that are in direct contact with an electrolyte; as shown by the pyroelectric and piezoelectric examples in Fig. 1. Triboelectric charges are produced as a result of a frictional contact between two materials which become electrically charged; these are typically used as motion harvesting tribo-electric nanogenerators (TENGs) which are electrically connected to an electro-chemical cell. The thermoelectric effect generates charge from a thermal gradient between two dissimilar conductors due to the Seebeck effect and is also typically used as a harvesting device which is connected to an electro-chemical cell. We will see that in some cases hybrid approaches are utilised that use more than one of the harvesting mechanisms shown in Fig. 1 or employ additional charge generation mechanisms, such a solar harvesting and photo-generated carriers. Table 1 provides a summary of the electro-chemical applications, harvesting materials and modes of operation, and

Vana Adamaki

Vaia Adamaki holds a diploma in Applied Physics and a MSc in Material Science and Technology and completed her PhD in 2014 at the University of Bath. Her PhD work was on the electrical and mechanical properties of Ti-suboxides and fibres for sensing and energy applications and now she focuses on finding efficient electrodes for water splitting.

Hamideh Khanbareh

Hamideh Khanbareh was awarded her PhD in Aerospace Engineering from Delft University of Technology in June 2016. She started a new role as a Prize Fellow in the Materials and Structures Research Centre within the Department of Mechanical Engineering, in University of Bath since September 2016. Her main research interests are in designing novel electro-ceramic–polymer composites for piezo- and pyroelectric sensing/energy harvesting applications. Her research includes experimental synthesis, characterisation as well as analytical and numerical modelling.

Chris R. Bowen

Christopher Rhys Bowen has a BSc degree in Materials Science from the University of Bath (1986–1990) and a DPhil from the University of Oxford (1990–1993). Post-doctoral work was at Tecnische Universität Harburg-Hamburg and University of Leeds (1994–1996). He was Senior Scientist at the Defence Evaluation and Research Agency from 1996–1998. He joined Bath as a Lecturer in 1998 and is now Professor of Materials and ERC Advanced Investigator, ERC Grant Agreement No. 320963 on Novel Energy Materials, Engineering Science and Integrated Systems (NEMESIS). Research includes energy harvesting, ferroelectrics and functional ceramics.

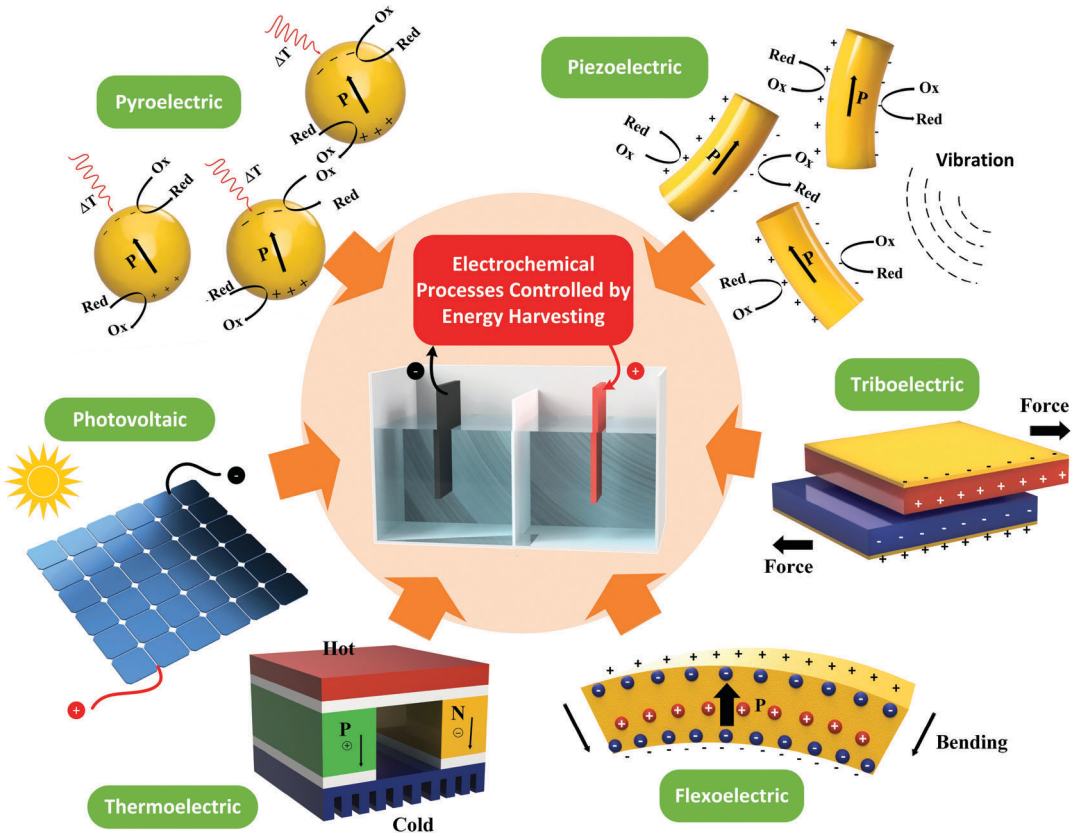

Fig. 1 Pyro-electric (temperature cycles), thermo-electric (temperature gradients), piezo-electric (strain), tribo-electric (motion), flexo-electric (strain gradient) and photovoltaic (solar excitation) charge generation mechanisms which are used to control electro-chemical reactions. The thermoelectric and triboelectric approaches typically use external devices, while the pyroelectric, piezoelectric and photovoltaic mechanisms can utilise external devices or particulates that are in direct contact with the electrolyte; as shown in upper images.

we will refer to this table throughout the review. The interaction of the harvesting material or device with electro-chemical systems will now be described, and their potential applications. Finally, potential future directions will be explored.

2. Pyro-electro-chemistry

2.1 Pyro-electro-chemical water splitting

The emission of CO_2 has been a significant contributor to global warming and climate change. As a result, renewable and alternative energy sources have become one of the primary topics of interest at a global level. Hydrogen fuel, is one of the most promising energy conversion technologies due to its high energy density and low greenhouse gas emission. Today, over 90% of hydrogen is produced from fossil fuels and biomass which produces greenhouse gases as a byproduct.[16] As an alternative, hydrogen production from clean and renewable resources has gained interest over recent decades. Water splitting, or electrolysis, by electricity or light (solar energy) is one of the most convenient ways of addressing this problem.[17–19] In order to trigger electrolysis and produce hydrogen gas, the overall potential difference between the anode and cathode is critical and, thermodynamically, the necessary potential difference is at least 1.23 V. Eqn (1) and (2) provide the minimum electrode potential for electrolysis at pH = 0. However, an excess energy, termed an overpotential, is required to overcome activation energy barriers during the reaction. Additional factors are that some of the products may catalytically reconvert to water, oxygen may oxidise the anode, and a double layer capacitance may be formed.

$$\text{Anode: } E = -1.23 \text{ V} \quad (1)$$

$$\text{Cathode: } E = 0.00 \text{ V} \quad (2)$$

According to Faraday's law of electrolysis, the mass of the substance produced by electrolysis is proportional to the quantity of carriers. This is expressed by eqn (3), where m is the mass of the substance, Q is the total electric charge passed through the substance, F is the Faraday constant, M is the molar mass of the substance and z is the valence number of ions.

$$m = [Q \cdot M]/F \cdot z \quad (3)$$

Hence, in addition to the critical potential to initiate the reaction, the available charge plays an important role in determining the amount of hydrogen that can be produced.

Table 1 Electrochemical applications, performances, employed materials and output form achieved by the utilisation of the pyro-, piezo-, flexo- tribo-electric and photovoltaic effects

Electro-chemical application	Primary electro-chemical mechanism	Energy har-vesting route	Primary material(s) used	Energy source for harvesting	Configuration of harvester relative to electro-chemical reactor	Short-circuit current (I_{sc}), open-circuit (U_{oc})			Electrical output (direct: (AC pulse) rectification/ transformation or indirect: stored in the super-capacitor/battery)	Ref.
						I_{SC}	U_{OC}	Condition		
Water Splitting	Anode: $4OH^- \rightarrow 2H_2O + O_2 + 4e^-$	Pyro-electric effect	PZT	Thermal	External	5 μA	4 V	Working freq. 0.1 Hz	Rectification and capacitor	20
	$2NaCl \rightarrow 2Na^+ + Cl_2 + 2e^-$		$BaTiO_3$	Thermal	Internal	—	—	—	—	23
	Cathode: $4H^+ + 4e^- \rightarrow 2H_2$		$PbTiO_3$ (theoretical)	Thermal	Internal	—	—	—	—	28
		Piezo-electric effect	ZnO/$BaTiO_3$	Water wave	Internal	—	—	Ultrasonic wave vibration	Transformation	49
			PMN–PT	Vibration	Internal	—	—	0.01 to 0.08 ppb/oscilla-	Transformation	52
			PZT-5	Vibration	External	—	12 V	tion	Rectification	54
			ZnO	Water wave + light	Internal	—	2 V	46.2 Hz/0.07N Ultrasonic wave vibration + xenon arc lamp (100 mW cm^{-1})	Transformation	55
		Tribo-electric effect	PA-PFA	Mechanical energy	External	0.06 mA	110 V	—	Li-ion battery	97
			Gold–Kapton	Flowing		1 mA	240 V	600 rmp	Supercapacitor	96
			TiO_2 Nanowire/ graphite Cu-PTFE	kinetic energy Wind		0.1 mA 1.5 mA	150 V 15 V	Wind speed of 15 m s^{-1} 500 rmp	Rectification Rectification	99 103
			ITO-PTFE	Biokinetic energy Linear motor		0.12 mA	200 V	60 N	Li-ion battery	101
		Thermo-electric effect	$FeSO_4$, HI	Solar energy	External	—	2 V	Light of wavelength from	AC pulse	178,179
			Carbon	Heat water bath	External	2 mA	200–	4k to 6k Å, Temp. gradient	AC pulse	180
			Silicon photo-electrode	Solar energy Heat water bath	External External	— —	1200 mV 350 mV	of 150 °C Hot side: 35 to 55 °C, cold	AC pulse AC pulse	181 182
			TiO_2 nanotube arrays				0.5 V	side: room temp Temp. gradient of 10 °C Hot side: 70 °C		
		Photovoltaic effect	GaInP/GaAs/Ge	Solar simulator	External	~160 mA	~2.2 V	150 W Xenon lamp	Direct	197
			InGaP/GaAs/ GaInNAsSb			~185 mA	3.21 V	550 W Xenon lamp		200
Degradation and water treatment	Anode: $2Cl^- \rightarrow Cl_2 + 2e^-$	Pyro-electric effect	$LiTaO_3$	Thermal	Internal	—	—	32 min per cycle	Direct	31
	$h^+ + OH^- \rightarrow {}^{\bullet}OH$		$LiNbO_3$	Thermal	Internal	—	—	32 min per cycle	Direct	31
	M (Metal) $\rightarrow M^{n+} + ne^-$		$BaTiO_3$–Pd particle	Thermal	Internal	—	—	—	Direct	32
				Thermal	Internal	—	—	27 to 38 °C per cycle	Direct	33
			$BiFeO_3$	Thermal	Internal	—	—	30 to 47 °C per cycle	Direct	34
	Cathode: $2H^+ + 2e^- \rightarrow H_2$		$BaTiO_3$	Thermal	Internal	—	—	22 to 62 °C per cycle	Direct	35
	$O_2 + e^- \rightarrow O_2^-$		ZnO	Thermal + mechanical	External	—	—	—	Rectification	37
			PZT + PDMS-PET							
	$Cu^{2+} + 2e^- \rightarrow Cu$	Piezo-electric effect	$BaTiO_3$	Water wave	Internal	—	—	Ultrasonic wave vibration	Transformation	57
	$nH_2O + ne^- \rightarrow n/2\ H_2 + nOH^-$		PZT	Water wave	Internal	—	—	Ultrasonic wave vibration	Transformation	58
			$BaTiO_3$/metal ions	Water wave	Internal	—	—	Ultrasonic wave vibration	Transformation	59
			ZnO	Vibration + light	Internal	—	—	1 Hz/1 cm of vibration &	Transformation	61
			$ZnSnO_3$	Stress + light	Internal	—	—	50 W/313 nm	Transformation	62
			$Zn_{1-x}SnO_3$	Stress + light	Internal	—	—	0.29–0.94 GPa stress & 15	Transformation	63
			CuS/ZnO	Stress + light	Internal	—	—	W/254 nm	Transformation	64
			Ag_2O/ZnO	Stress + light	Internal	—	—	0.4–0.6 GPa stress & 30 W/	Transformation	65
			Ag/ZnO	Stress + light	Internal	—	—	330 nm	Transformation	66

Table 1 (*continued*)

Electro-chemical application	Primary electro-chemical mechanism	Energy harvesting route	Primary material(s) used	Energy source for harvesting	Configuration of harvester relative to electro-chemical reactor	Short-circuit current (I_{sc}), open-circuit (U_{oc})			Electrical output (direct: (AC pulse) rectification/ transformation or indirect: stored in the super-capacitor/battery)	Ref.
						I_{SC}	U_{OC}	Condition		
								Ultrasonic probe (200 W) & solar light (500 W)		
								Ultrasonic probe (200 W) & UV light (50 W)		
								Ultrasonic probe (200 W) & solar light (500 W)		
		Tribo-electric effect	Al-PTFE	Linear motor	External	—	30 V	—	Rectification	104
			ITO/SiN-PDMS	Mechanical energy		~85 nA	2.5 V	Working freq. of 1 Hz	Rectification	105
			PET-PDMS	Mechanical energy		0.2 μA	12 V	—	Li-ion battery	37
			TiO_2 Nanowire/ PTFE	Wastewater wave		~1.2 μA	~7 V	Wave speed of 1.4 m s^{-1}	Rectification	107
				Water wave		0.12 mA	270 V	Working freq. of 2 Hz	Rectification	108
			ITO-PTFE	Flowing		0.45 μA	2 V	650 rmp	Transformation/rectification	106
			Copper-Kapton	kinetic energy		69.9 μA	845.6 V	Vibration freq. of 2.08 Hz	Transformation/rectification	110
			Copper-Kapton	Linear motor		13 mA	3 V	450 rmp	Transformation/rectification	114
			Copper-Kapton	Motor		3.5 mA	10 V	Water flow rate of 3 L min^{-1}	Transformation/rectification	118
			Copper-FEP	Flowing waste-water		15 μA	50 V		Capacitor	117
			Al-PTFE			8 mA	16 V	Wind speed of 10 m s^{-1}	Supercapacitor	116
			Copper-FEP	Ambient		0.56 mA	793 V	1500 rmp	Rectification	111
			Al-PTFE	natural wind		1.2 mA	1300 V	Vibration freq. of 3 Hz	Rectification	112
			Copper-PTFE	Water		0.2 μA	600 V	Vibration freq. of 4 Hz	Transformation/rectification	113
			Alo-Kapton	Vibration				1000 rmp		
				Vibration						
				Vibration						
		Photovoltaic effect	GaInP/GaAs/Ge	Solar simulator	External	~6.5 mA	1.34 V	1 sun density spectrum	Direct	201
			Zinc			150 mA	—	~240 W silicon cells	Direct	214
Corrosion protection	By generating charge, the surface of the protected cathode is below the corrosion potential.	Pyro-electric effect	PVDF + PTFE	Thermal + mechanical	External				Rectification	38
		Piezo-electric effect	PVDF + PTFE	Thermal + mechanical	External				Rectification	38
		Tribo-electric effect	Copper–Kapton	Motor	External	32.1 μA	310 V	1000 rmp	Rectification	120
			Nylon-PVDF	Motor		51.4 μA	1008 V	Working freq. of 7.5 Hz	Capacitor	122
			Ag-PET	Water wave		5 μA	75 V	Wave speed of 0.2 m s^{-1}	Supercapacitor	121
			PET-PDMS	External stimulation		130 μA	500 V	Working freq. of 1 Hz	Rectification	123
			Kapton-PTFE			13 μA	230 V	Working freq. of 1.25 Hz	Rectification	119
			Al-PTFE	Water wave		0.42 μA	8 V	Vibration freq. of 3 Hz	Rectification	38
			PVDF-PPy Nano-wire	Vibration		33.7 μA	351 V	Working freq. of 8 Hz	Rectification	125
				Motor		30 μA	1000 V	Working freq. of 5 Hz	Capacitor	124
			Gum wrapper-PVDF	Motor						
Self-charging power cells	Polyethylene separator of a conventional Li battery is replaced with a	Piezo-electric effect	PVDF	Compressive strain	Internal	—	—	Compressive strain	Transformation	75
			CuO/PVDF	Compressive strain	Internal	—	—	18 N, 1 Hz	Transformation	76
			mesoporous PVDF	Compressive strain	Internal	—	—	22–34 N, 1.8 Hz	Transformation	78
			Highly	Compressive strain	Internal	—	—	141, 282, 423 mJ, 1 Hz	Transformation	77
			porous PVDF	Compressive strain	Internal	—	—	10 N, 1.5 Hz	Transformation	79

Table 1 (*continued*)

Electro-chemical application	Primary electro-chemical mechanism	Energy harvesting route	Primary material(s) used	Energy source for harvesting	Configuration of harvester relative to electro-chemical reactor	Short-circuit current (I_{sc}), open-circuit (U_{oc})			Electrical output (direct: (AC pulse) rectification/ transformation or indirect: stored in the super-capacitor/battery)	Ref.
						I_{SC}	U_{OC}	Condition		
	piezoelectric material. Under the compressive strain the produced piezo-electric field of the piezoelectric separator drives charges from the cathode to the anode, thereby recharging the power cell		PVDF-PZT	Compressive strain	Internal	—	—	9.8–18.8 N finger tapping	Transformation	80
			PVDF-ZnO	Compressive strain	Internal	—	0.31 V	70 N, 5 Hz	Transformation	82
			P(VDF-TrFE) foam	Compressive strain	Internal	14.5 μA	0.023 V	0.3 Hz finger tapping	Transformation	85
			Li-alloyed Si (piezo-resistive)	Compressive strain	Internal	—	—	Deformation of Si nano-particles during lithiation (1.7 GPa)	Transformation	84
			$BaTiO_3$ nanoparticles							
Electro-deposition & oxidation	Generated charges can reduce the metal cations to form a coherent metal coating on an electrode	Tribo-electric effect	Kapton-PMMA	Vibration	External	6 μA	110 V	—	Rectification	126
			PTFE-PPy	Shaker motor		68 μA	200 V	Working freq. of 10 Hz	Supercapacitor	128
		Thermo-electric effect	PEDOT-PSS	Heat	External	—	50 mV	Temp. gradient of 1 K	Supercapacitor	226
Chemical sensor	Using a modifying agent in the power source to detect chemicals.	Tribo-electric effect	Au nanoparticles-PDMS	Controlled force	External	63 μA	105 V	Force of 50 N, freq. of 5 Hz	Rectification	132
			Al-PA	Liquid dripping		—	~70 V	Water drop	AC output	134
			PVDF-nylon	Vibration		81 μA	1163 V	Triggering freq. of 5 Hz	Rectification	145
			β-CD/TiO_2-PTFE	Water wave		80 μA	70 V	Wave speed of 1.4 m s^{-1}	Rectification	107
			Al-PTFE	Vibration		33 μA	116 V	Force of 60 N, freq. of 1 Hz	AC output	130
			Cu-FEPAAO-PTFE	Blowing		~4 μA	~17.5 V	Blowing speed of 2 m s^{-1}	AC output	133
			Al-melamine	Water		~0.2 μA	~150 V	Water flow rate of 3 L	Rectification	131
			Al-PTFE	External stimulation		6.18 μA	23.8 V	min^{-1}	AC output	144
			Copper-PZT			1.86 μA	33.7 V	Working freq. of 3 Hz	AC output	143
				External force		3.7 μA	—	Working freq. of 5 Hz	AC output	146
				External agitation				—		
		Thermo-electric effect	Al-PTFE gelatin/ glycerol	Aspiration & dispensing of the pipet from the solution		—	~0–0.5 mV	Aspiration of the solution by the pipet tip and temp. gradient from −4 to 64 °C	Capacitor	224
Electro-chromic	Injected charges can energize the electro-chemical redox reactions.	Tribo-electric effect	ITO/PET-PDMS	Wind	External	45 μA	140 V	Wind speed of 16.1 m s^{-1}	Rectification	139
			POM-PTFE	Force		434.3 μA	236.8 V	Force of 400 N, freq. of 5	Rectification	140
			Fluorocarbon-ITO	Vibration		100 μA	200 V	Hz	Capacitor	137
			Copper-PDMS	Motor		~0.15 μA	~3.75 V	Working freq. of 10 Hz	AC output	141
			Copper-PTFE	Finger-induced strain		3.5 μA	90 V	15 N, 3 m s^{-2}	Rectification	142
			PDMS-human skin	Human motion		3.1 μA	56 V	4 Hz	Rectification	138
								—		
		Thermo-electric effect	PEDOT-PSS	Heat	External	—	50 mV	Temp. gradient of 1 K	Supercapacitor	226

Table 1 (*continued*)

Electro-chemical application	Primary electro-chemical mechanism	Energy har-vesting route	Primary material(s) used	Energy source for harvesting	Configuration of harvester relative to electro-chemical reactor	Short-circuit current (I_{sc}), open-circuit (U_{oc})			Electrical output (direct: (AC pulse) rectification/ transformation or indirect: stored in the super-capacitor/battery)	Ref.
						I_{SC}	U_{OC}	Condition		
Biological related	Bone healing	Piezo-electric effect	Collagen	Deformation	Internal	—	—	—	Transformation	86
	Ion pumping in bio membranes	Flexo-electric effect		Deformation	Internal	—	—	—	Transformation	158 and 159
Self-healing structures	By mimicking the ability of biological struc-tures to redis-tribute their structural mass in response to dynamic loads	Piezo-electric effect	PVDF-HFP & PZT	Deformation	Internal	—	—	—	Transformation	89
Ice forming and polymer patterning	Local electric field leads to the formation of the ice-like nuclei or electrowetting effect	Pyro-electric effect	$LiTaO_3$	Electric field	Contact	—	—	—	—	41
			$SrTiO_3$	Electric field	Contact	—	—	—	—	41
			PVDF	Electric field	Contact	—	—	—	—	42
			Amino acid crys-tals	Electric field	Contact	—	—	—	—	43 and
				Thermal contact	Contact	—	—	—	—	45
			$LiNbO_3$							47 and 48
Other applications	Thermoelectric polymer with large Seebeck coefficient	Thermo-electric effect	PEDOT:PSS	Peltier heater	External	—	~5 mV	Temp. gradient of 1, 2.5 and 3.5 K, relative humidity 100%	AC pulse	184

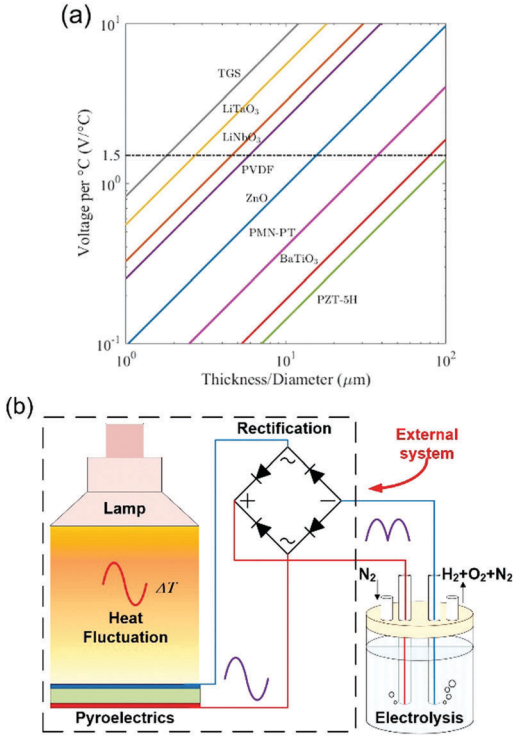

Fig. 2 Pyroelectric water splitting. (a) Open circuit voltage generated for 1 °C change *vs.* pyroelectric film thickness. Critical potential for electrolysis is indicated as 1.5 V; $\Delta V = [p/(\varepsilon_{33}^{T})]\cdot h\cdot\Delta T$. Reproduced from ref. 20. Copyright (2017) with permission from Elsevier. (b) Schematic of a pyroelectric used as an external power source for water splitting.

Pyroelectric energy harvesters, as a potential energy source, have been used in an effort to split water. The pyroelectric charge (Q) generated for a temperature change (ΔT) is given by,

$$Q = p\cdot A\cdot\Delta T \quad (4)$$

where p is the pyroelectric coefficient (C m^{-2} K^{-1}) and A is the surface area. Xie *et al.* analysed a range of pyroelectric materials and geometries for water electrolysis to determine the minimum material thickness to generate a critical potential (1.23–1.5 V) to initialise water decomposition and maximise the charge and mass of hydrogen production (eqn (3)).[20] This is shown in Fig. 2(a) where the potential ΔV developed across a pyroelectric of thickness, h, is given by

$$\Delta V = [p/(\varepsilon_{33}^{T})]\cdot h\cdot\Delta T \quad (5)$$

where ε_{33}^{T} is the material permittivity at a constant stress. It is interesting to note that for a given material the charge is proportional to the surface area (eqn (4)) while the electric potential (eqn (5)) is proportional to its thickness, indicating a need to tune the geometry of the pyroelectric elements. Using this analysis, Xie *et al.* demonstrated experimentally that a lead zirconate titanate (PZT) plate, when combined with rectification of the alternating current to provide a unipolar output, was able to harvest heat fluctuations and generate a sufficient electric potential difference for water splitting. In this case the pyroelectric water splitting was achieved by positioning the pyroelectric material outside of the water and the material was used as an external charge source, as in Fig. 2(b) and further experimental details are summarised in Table 1. A patent on pyroelectric water splitting has also been filed which describes a device that combines a liquid based temperature control device, two gas chambers and a pyroelectric material that is in partial contact with water to undergo reduction–oxidations (Red–Ox) reactions when pyroelectric charges are generated on its surface during temperature changes.[21] Similarly, Cherkouk *et al.* used a finite element method to simulate a pyroelectric system that converted periodic heating from laminar water flow into pyroelectric charges and further proposed it can be converted into chemical energy *via* water splitting.[22]

Rather than using the pyroelectric materials as an external charge source, Belitz *et al.* recently developed a pyroelectric water splitting system where a $BaTiO_3$ single crystal powder were brought into direct contact with distilled water in a polystyrene container which was subjected to a cyclic temperature change from 40 °C to 70 °C.[23] A specially designed coulometric solid electrolyte detector indicated that 300 Vol.-ppb hydrogen was generated after a small number of pyroelectric cycles. The advantage of this approach, compared to using a bulk materials, is that using finely dispersed pyroelectric particulates enables the area of the pyroelectric to be greatly increased, and therefore increase the available charge for hydrogen production (eqn (3) and (4)).

Materials that exhibit high pyroelectric coefficients are typically ferroelectric that have a switchable polarisation, and the direction of polarisation can affect its surface stoichiometry and electronic structure, and therefore adsorption energy. The modification of ferroelectric surfaces to control surface chemistry and enhance catalytic properties has been studied in the areas of adsorption, desorption and photo-catalysis.[24,25] In recent papers,[25,26] Kakekhani *et al.* proposed a pyro-catalytic reaction that is activated by cycling a material between two ferroelectric polarisation states (one surface state with a strong adsorption potential and the other surface state with a strong desorption potential). Density functional theory (DFT) indicated that ferroelectric $PbTiO_3$ can effectively convert SO_2 to SO_3 and can be used to control binding energies and hence decompose NO_x into N_2 and O_2 by using a positive and negative polarisation. In addition, the potential of catalysing the partial oxidation of methane to methanol was reported.[27] DFT was also used examine the potential of pyroelectric materials for water splitting.[28] In the modelling approach, the surface of a ferroelectric lead titanate ($PbTiO_3$) material was cycled between its low temperature ferroelectric state and high temperature para-electric phase by thermally cycling above and below its Curie temperature (T_c). In the lower temperature ferroelectric and polarised state, H_2O molecules are thought to dissociate on the negatively poled surface of the lead titanate to produce bound atomic hydrogen (see blue region of Fig. 3 where $T < T_c$). When the material is heated to the higher temperature non-polarised and para-electric phase, the hydrogen atoms recombine to form weakly bound H_2, thereby creating a clean surface that is ready for the next thermal cycle (see red region of Fig. 3 where $T > T_c$). This provides an

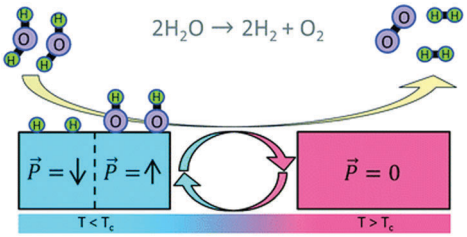

Fig. 3 Water splitting by thermal cycling between a polarised (left, blue) and para-electric (red, right) surface of a pyroelectric material. Two water molecules are dissociated on the polarised surface to produce bound atomic hydrogen and when the surface is switched to the para-electric phase, the H atoms recombine to form weakly bound H_2. Reproduced from ref. 28 with permission from The Royal Society of Chemistry.

intriguing approach to harvest thermal fluctuations to produce hydrogen, although no experimental evidence has been reported to date.

2.2 Pyro-electro-catalysis

The demand for clean water continues to rise due to worldwide growth in our population and agriculture, and increased industrial development. When heavy metals, bacteria and organic dyes enter our water, it can be difficult to treat and can lead to health and environmental problems and therefore new technologies for their removal has become desirable.[29] In this regard, the use of pyro-electro-catalysis, which combines the pyroelectric effect and electro-chemical oxidation–reduction reactions, has been studied and used for the disinfection of bacteria and decomposition of a variety of toxic and hazardous organic compounds in aqueous environments.

2.2.1 Pyro-electro-chemical disinfection. Wiesner[30] was first to propose that the pyroelectric effect has the potential to drive a reduction–oxidation reaction, since an electrical charge and a potential difference is developed across a material as a result of a temperature change (eqn (4) and (5)). The anticipated voltage waveform from a thermally cycled pyroelectric material was simulated by an arbitrary function generator (1.5 V at 4 Hz) and the change in the colour of an electrolyte with time demonstrated that it is possible to reduce Fe^{3+} to Fe^{2+}. In order to experimentally prove the concept of pyro-electro-catalysis, a pyroelectric lithium tantalate ($LiTaO_3$) wafer with a pyroelectric coefficient of 230 μC m^{-2} K^{-1} was thermally cycled under UV light at 4 Hz; however, no experimental results were shown. Later, Gutmann *et al.* studied the application of pyro-electro-catalysis for disinfection applications. They utilised thermally excited pyroelectric crystals in an aqueous solution to create reactive oxygen species (ROS) to disinfect *Escherichia Coli* (*E. coli*) bacteria.[31] Nano- and micro-crystalline lithium niobate ($LiNbO_3$) and $LiTaO_3$ powder were placed into an aqueous solution and subjected to a temperature cycle between 20 and 45 °C. The mechanism of disinfection is shown in Fig. 4, where in (a) the material is initially in equilibrium and there are bound surface charges (blue circles) due to the spontaneous polarisation ($\vec{P}$) of the ferroelectric $LiTaO_3$ (shown as red circles). When the material is heated in Fig. 4(b), the polarisation of the pyroelectric

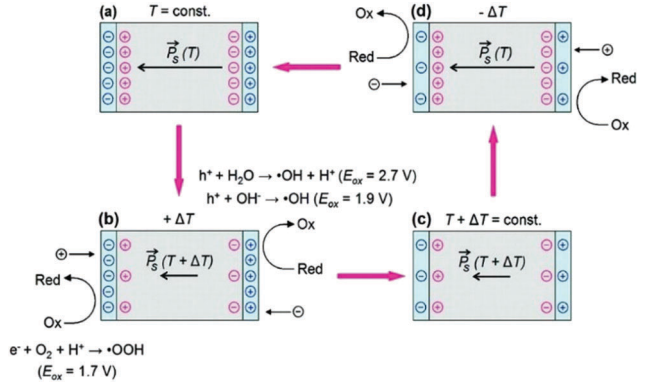

Fig. 4 The pyro-electro-catalytic cycle due to thermal cycling of a pyroelectric crystal in aqueous conditions and subsequent surface reactions. (a) and (c) are the equilibrium condition at different temperatures, while (b) and (d) show the surface potential due to a transient imbalance between polarisation (red circles) and screening charges (blue circles). If the surface potential in (b) and (d) exceeds the oxidation potentials, surface-adsorbed molecular species can undergo redox reactions, resulting in formation of reactive oxygen species (ROS). Reprinted with permission from ref. 31. Copyright (2012) American Chemical Society.

is reduced so that some of the bound charge is now free to take part in reduction–oxidation reactions (Red–Ox) until the excess (free) charges are consumed in Fig. 4(c). When the material is subsequently cooled the polarisation of the material increases and charges move to the surface to balance the uncompensated screening charge carriers, leading to further Red–Ox reactions. It should be noted from Fig. 4 that the polarity of the charges moving to each surface changes depend on whether the material is undergoing a heating cycle (a polarisation decrease) or a cooling cycle (a polarisation increase). To demonstrate the potential of pyroelectric disinfection, Fig. 5 shows vitality staining of bacterial cultures which show the disinfection of the *E. coli* bacterial cells due to the pyroelectric effect of $LiTaO_3$ powders; the *E. coli* were killed after thermal treatment of $LiTaO_3$ for three hours.

In 2015 Benke *et al.*[32] reported an enhanced disinfection process, which was assisted with the use of palladium nanoparticles on the pyroelectric particle surfaces. Barium titanate ($BaTiO_3$) nanoparticles of 100 nm in size where coated with 40 nm palladium (Pd) nanoparticles. The mechanism is shown

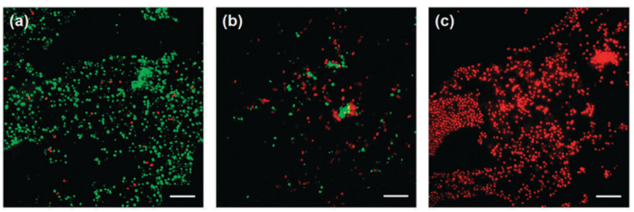

Fig. 5 Vitality staining of bacterial cultures. Fluorescence microscopy images of LIVE/DEAD stains of *E. coli* cultures not subjected to thermal treatment (a), after thermal treatment for 2 h in the presence of $LiTaO_3$ (5–10 μm) (b), and after 1 h thermal treatment in the presence of $LiTaO_3$ (<5 μm) (c). Reprinted with permission from ref. 31. Copyright (2012) American Chemical Society.

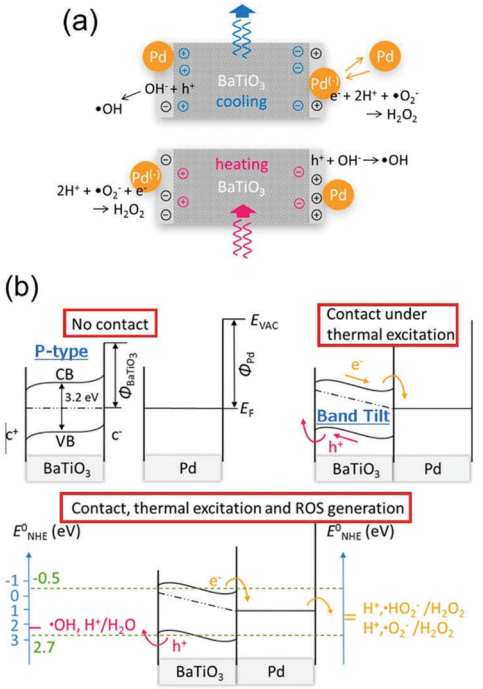

Fig. 6 (a) Schematic of reactive oxygen species (ROS) generation driven by the pyro-electro-chemical effect assisted by palladium nanoparticles.[32] (b) Energy level diagrams and reactive oxygen species (ROS)-generating charge transfer due to thermal excitation of pyroelectric barium titanate. Redox potentials between palladium nanoparticles, barium titanate, and neutral aqueous surrounding relative to standard hydrogen electrode are compared for selected species. Adapted with permission from ref. 32. Copyright (2015) American Chemical Society.

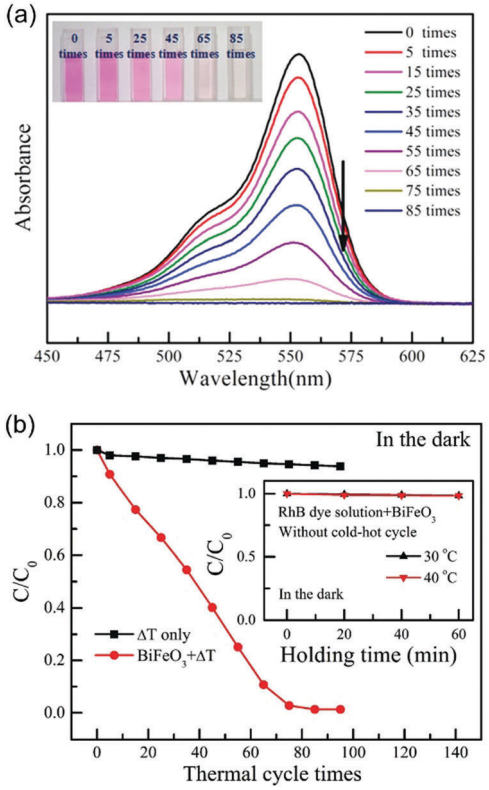

Fig. 7 (a) UV-vis spectra of the Rhodamine B (RhB) solution with increasing numbers of thermal cycles (from 27 °C to 38 °C) using $BiFeO_3$ nanoparticles as the pyro-electro-catalyst. The inset shows the colour change of the RhB dye solution after increasing number of cold–hot cycles. (b) Pyro-electro-catalytic RhB dye degradation after increasing number of thermal cycles (from 27 °C to 38 °C) with or without $BiFeO_3$ nanoparticle pyro-electro-catalyst. For comparison, the inset shows the RhB dye degradation with $BiFeO_3$ catalyst after being held at a constant temperature. Reproduced from ref. 33 with permission from The Royal Society of Chemistry.

in Fig. 6(a) where again heating and cooling cycles lead to free surface charges being produced on the polarised material surface, which can contribute to Red–Ox reactions. Due to the small particle size, the surface potential generated by the $BaTiO_3$ nanoparticles from pyroelectric effect is lower than the voltage needed for reactive oxygen species generation (see eqn (5)). However, in their energy band model, which is shown in Fig. 6(b), the pyroelectric $BaTiO_3$ particle was assumed to be a p-type semiconductor and the Fermi level of $BaTiO_3$ was at the mid-band gap (Fig. 6(b), upper left). The band of $BaTiO_3$ is thought to tilt due to the internal electric field that is generated by a change in temperature and the pyroelectric effect (Fig. 6(b), upper right). As the Pd nanoparticles are in contact with the $BaTiO_3$ particles, electrons (e^-) are able to transfer into the Pd particles and the holes (h^+) into the valence band of $BaTiO_3$ to become a source of $^\bullet$OH radicals (Fig. 6(b), lower image). Hence Benke *et al.* assumed that the $^\bullet$OH generating reaction, which improved disinfection, was strongly dependent on the enhanced charge transfer between the Pd and $BaTiO_3$ nanoparticles.

2.2.2 Pyro-electro-chemical degradation. In a similar approach to pyroelectric disinfection, bismuth ferrite ($BiFeO_3$) nanoparticles have been used to degrade an organic dye solution of Rhodamine B (RhB) using the pyroelectric effect. The process was shown to achieve a 99% degradation efficiency after 85 thermal cycles for a temperature cycle from 27 °C to 38 °C.[33] The inset of Fig. 7(a) shows the colour change of the RhB dye solution with an increasing number of cold–hot cycles and the degradation efficiency is shown in Fig. 7(b) along with a comparison of the response of a control sample in the dark and at constant temperature. Inspired by this research, the same group investigated the potential of pyroelectric dye degradation using lead-free/non-toxic $BaTiO_3$ nanofibers.[34] The decomposition of RhB was again high, up to 99%, when the material was subjected to 72 cold–hot cycles from 30 °C to 47 °C. In addition, there was no significant decrease in the pyro-electro-catalytic activity after five dye decompositions; thereby indicating the potential of the material for long-term operation. Additional pyroelectric materials have also been explored for degradation applications; for example ZnO nanorods exhibited a high pyro-electro-catalytic activity for RhB and attained a 98.15% decomposition after 27 thermal cycles between 22 °C and 62 °C.[35] A patent for an energy and substance conversion device that uses pyroelectric materials to produce cleavage products from fluids has also been filed.[36]

2.2.3 Hybrid pyro-electro-chemical energy cells. For energy harvesters coupled to electro-chemical systems, several hybrid

energy generators have been investigated in order to increase the reaction rate and the amount of available charge to contribute to electro-chemical reactions. In particular, the combination of pyro-electric, piezoelectric and triboelectric nanogenerators (TENGs) has been explored and devices based on TENGs will be described in more detail in Section 4. Yang *et al.* was first to demonstrate a hybrid energy cell comprised of an anodic aluminium oxide template with a polydimethylsiloxane nanowire array as a tribo-electric nanogenerator and a lead zirconate titanate (PZT) film as the pyroelectric energy harvester.[37] In this case the generator was used as an external charge source rather than particulates dispersed in a solution. Energy was harvested from a pyroelectric thermal cycle (heating from 295 K to 309 K in 100 s and then cooling to 309 K in 100 s) along with mechanical energy from the ambient environment using a TENG to degrade methyl orange. Fig. 8(a) shows a schematic of the self-powered hybrid cell showing the combined pyro- and tribo-electric nanogenerators (NGs), the rectification bridge which acts to maintain the polarity of the alternating current (AC) output and the electrodes connected to the methyl orange solution; a lithium battery is also present to provide additional electrical energy storage. The degree of methyl orange degradation was 80% after 144 hours of operation with an observed colour change; see Fig. 8(b). A hybrid nanogenerator approach is also shown in Fig. 9(a), which used polyvinylidene difluoride (PVDF) as the active pyroelectric material and a patterned PTFE/Al combination as the triboelectric nanogenerator.[38] Since pyroelectric materials are also piezo-electric, the PVDF was also used and a piezoelectric harvester to harvest mechanical vibrations. Since all three mechanisms produce an alternating current under a cyclic temperature or stress, rectification was used to maintain a constant polarity at the steel cathode and carbon anode. In this example the potential produced was used to achieve self-powered cathodic protection and the Nyquist plot in Fig. 9(b) indicates that little or no rust layers are formed on the steel electrode surface compared to steel not connected to the nanogenerators.

Pyroelectric materials also have the potential to simply harvest temperature changes associated with exothermic or endothermic reactions. Industrial and lab-scale chemical processes can generate a large amount of waste heat and the low-grade nature of the heat and ease of dissipation makes is difficult to be harvested. Zhao *et al.* fabricated a flexible pyro-electric energy harvester, which consisted of ferroelectric PVDF sandwiched between two multi-walled carbon nanotubes electrodes. This system was demonstrated to harvest sufficient waste heat from chemical exothermic process for low power electronics.[39]

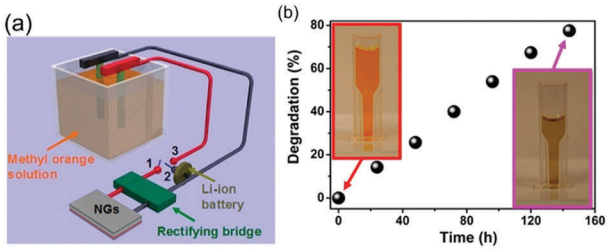

Fig. 8 Hybrid pyro- and tribo-electric energy cell for electro-catalytic oxidation and degradation of methyl orange. (a) Schematic of self-powered electro-degradation of methyl orange (MO). (b) Degradation and colour change of the methyl orange solution with time. Reprinted with permission from ref. 37. Copyright (2013) American Chemical Society.

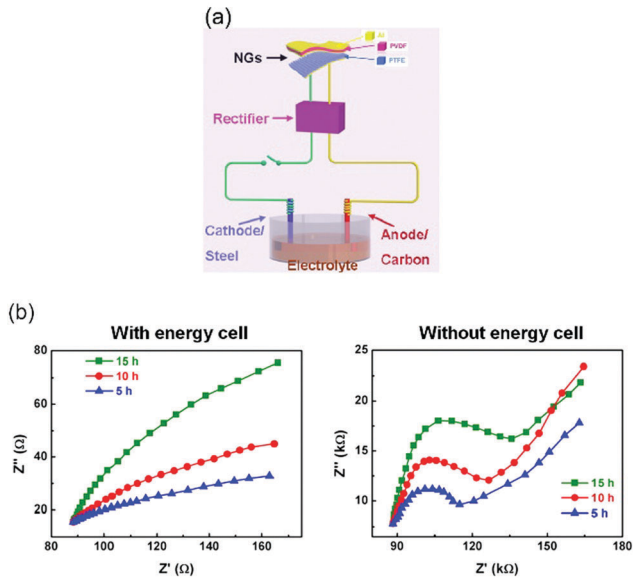

Fig. 9 (a) Schematic of hybrid self-powered cathodic protection system and (b) Nyquist diagrams of carbon steel electrodes after corrosion with and without hybrid the nanogenerator (energy cell). Adapted with permission from ref. 38. Copyright (2015) American Chemical Society.

2.3 Pyro-electric ice-formation and other applications

Beyond the reduction–oxidation reactions that have been described above, pyroelectric materials have also been used to control surface ice-formation, indicating potential use of charges generated during heating or cooling to control freezing behaviour. Control of the freezing temperature of super-cooled water is important in areas such as cell and tissue cryo-preservation and prevention of crop freezing. Electro-freezing[40] using electric fields on charged surfaces has been exploited for the formation of ice-like nuclei and enhance the freezing of super-cooled water. The use of electro-freezing on metallic surfaces is difficult since its electrical conductivity isolates the net effect of the electric field. Ehre *et al.* reported the use of pyroelectric materials to isolate the electric field since they are insulators (dielectrics) and the polarity of the surface can be manipulated by changing the polarisation direction.[41] Positively charged surfaces of pyroelectric $LiTaO_3$ crystals and $SrTiO_3$ thin films were shown to promote ice nucleation, while negatively charged surfaces were shown to inhibit ice nucleation and thereby reduce the freezing temperature. Fig. 10 shows optical microscopy images of water droplets and condensation on amorphous (top) and quasi-amorphous (bottom) films of $SrTiO_3$ at a variety of temperatures. The water was observed to freeze at a higher temperature of −4 °C on the quasi-amorphous (pyro-electric) film compared to −12 °C on the amorphous (nonpolar)

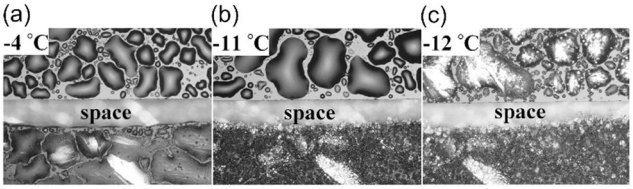

Fig. 10 Freeze point control using pyroelectric materials. Optical microscopy images of water drops condensed on non-pyroelectric amorphous (top) and pyroelectric quasi-amorphous (bottom) films of $SrTiO_3$ at various temperatures. Water freezes at −4 °C on the quasi-amorphous (pyroelectric) film and at −12 °C on the amorphous (nonpolar) film. From ref. 41. Reprinted with permission from AAAS.

film. In addition, it has been reported that polyvinylidene fluoride (PVDF) can be used as an ice repellent coating[42] and the strength of ice repellency can be increased by increasing the polarisation of the coating. Pyroelectricity has also been recently observed in nonpolar, centrosymmetric crystals of amino acids[43,44] which originates from the thin polar layer of hydrated α-glycine near its surface and this influences its freeing characteristics. With amino acid crystals, Ehre *et al.* found that ice nucleation can be close to 0 °C due to a relatively large pyroelectric effect.[45]

In a similar approach to tuning ice nucleation, pyroelectric materials have been used to pattern polymer films; and the reader is referred to a review by Coppola *et al.*[46] Xi *et al.* used $LiNbO_3$ (LN) to generate parallel charge patterns, and achieved self-assembly and patterning of a thin polymer film through an electro-hydrodynamic process.[47] By placing a hot polydimethylsiloxane (PDMS) stamp on a $LiNbO_3$ surface, it was possible to induce the formation of local pyroelectric charge by transferring heat from a patterned PDMS stamp to the pyroelectric $LiNbO_3$. The electrostatic stress generated from the patterned surface charge was able to drive the assembly of the thin polymer film into microarrays. A schematic of the process is shown in Fig. 11 where the hot stamp generates surface charges for assembly of solvents (a to b) or immersion in water for patterning (c to e). In addition, periodically poled pyroelectric crystals can lead to electrowetting effect and form liquid lenses on a surface in an electrodes-less and circuit-less manner.[48]

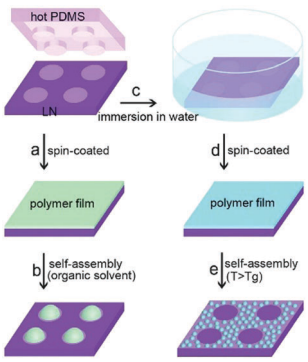

Fig. 11 Schematic showing the procedure of electrostatic charge patterning using hot micro-contact printing on $LiNbO_3$ (LN) substrate followed by self-assembly of thin polymer film. Reproduced from ref. 47 with permission from The Royal Society of Chemistry.

This provides scope for thermal scavenging for freezing/wetting, materials assembly and fabrication, and examples of harvesting for materials synthesis is described in the section on tribo-electric harvesting.

3. Piezo-electro-chemical effect

The direct conversion of mechanical energy into chemical energy, known as the piezo-electro-chemical (PZEC) effect, was first reported in 2010 by Hong *et al.*[49] In this work, the piezoelectric properties of the materials were used to achieve water splitting for hydrogen generation. Following this work, the piezo-electro-chemical effect was utilised for a number of other applications, such as water purification and self-charging power cells, either as the sole harvesting mechanism or used in a hybrid system to enhance the primary energy conversion. These approaches will now be described.

3.1 Piezo-electro-chemical water splitting

Hong *et al.* used piezoelectric ZnO microfibres and $BaTiO_3$ micro-dendrites immersed in water to produce H_2 by harvesting ultrasonic vibrations.[49] Fig. 12 shows the piezoelectric charges developed on a ZnO fibre surface as a consequence of being mechanically excited by ultrasonic waves; the conditions are summarised in Table 1. The resulting mechanical strain of the ZnO fibre changes its polarisation to create free surface charges that can contribute to Red–Ox reactions on the positive and negative surfaces of the piezoelectric fibre. This is shown in Fig. 12 where bending from ultrasonic excitation is thought to produce negative charges on the tensile face and positive on the compressive face to contribute to Red–Ox reactions.

To achieve water splitting the developed potential must be greater than the redox potential of water (eqn (1) and (2)) and potentials lower than 1.23 V will not participate in reactions to form H_2 and O_2. Starr *et al.*[50] used a single-crystal ferroelectric $Pb(Mg/3Nb_{2/3})O_3$–$32PbTiO_3$ (PMN–PT) cantilever in a sealed chamber that was strained using a computer controlled vibrator and linear actuator. Fig. 13 shows the experimental set up where deformation of the piezoelectric cantilever was achieved remotely *via* two encapsulated magnetic materials placed at the tip of both the cantilever beam and driving lever arm.

Following this work, Starr provided general guidance on approaches to exploit the piezoelectric properties of materials to initiate surface reactions.[51,52] Their fundamental analysis indicates that a high piezoelectric coupling coefficient and a low electrical conductivity are desired for enabling high

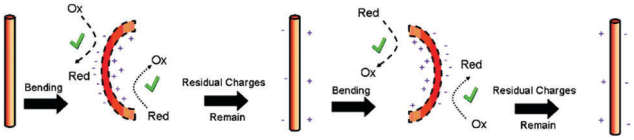

Fig. 12 Schematic of piezoelectric charges and Red–Ox reactions on a ZnO fiber surface through bending by ultrasonic vibration. Reprinted with permission from ref. 49. Copyright (2010) American Chemical Society.

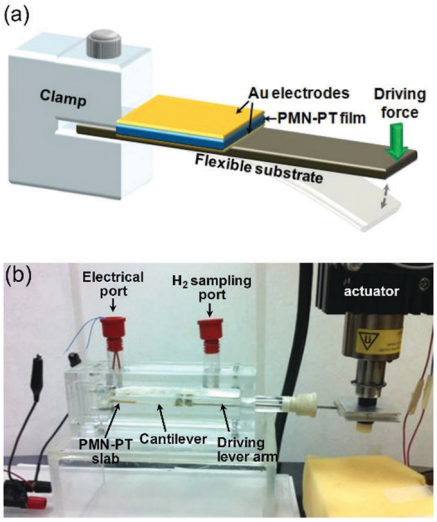

Fig. 13 Piezoelectric water splitting experimental setup: (a) flexible substrate for strain induction, a piezoelectric element for generation of piezoelectric potential and charge, and a clamp for securing the cantilever base. (b) Experimental setup and reaction apparatus used for studying piezo-catalysed hydrogen evolution from water. Reprinted from ref. 50, Copyright (2015), with permission from Elsevier.

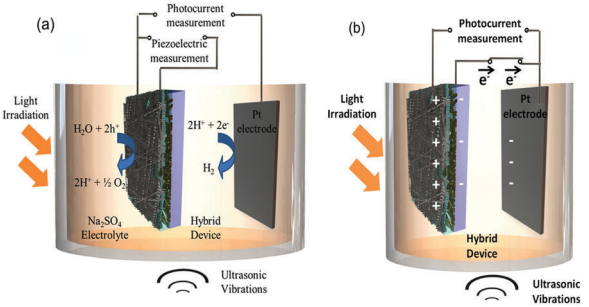

Fig. 14 Operation of the hybrid device (a) Individual piezoelectric and photocurrent measurement (b) Charge transfer during deformation of the piezoelectric and photo-catalytic electrode under ultrasonic vibration and light irradiation. Reprinted with permission from ref. 55. Copyright (2015) American Chemical Society.

electrochemical activity. Materials that could be used for such applications are PMN–PT, ZnO, $BaTiO_3$ and $PbTiO_3$; and many of the materials are shown in Fig. 2 for the pyroelectric analysis of Xie *et al.* The correlation between piezoelectric and pyroelectric properties is unsurprising since both originate from a change in polarisation with stress or temperature, respectively;[53] see Fig. 1. In an attempt to achieve a more flexible and inexpensive harvesting design that could utilize low vibration frequencies, rather than high frequency ultrasound, Zhang *et al.* proposed an indirect piezo-electro-chemical process for water splitting.[54] The device consisted of a piezoelectric bimorph cantilever and a water electrolysis system; the electrical output produced by mechanical vibrations was rectified and connected to an electrolyte to split water into hydrogen and oxygen. This design offered more flexibility and a high output voltage (approximately 12 V, see Table 1). The hydrogen production rate was 10^{-8} mol min^{-1} and approaches to enhance the production range include using a piezoelectric material with a higher piezoelectric coefficient (d_{ij}) and increasing the conductive ion concentration of the $NaHSO_4$ electrolyte solution. Other factors can include increasing area (A) and level of applied stress (σ); since $Q = d_{ij} \cdot A \cdot \sigma$.

The piezoelectric properties of materials have also been used in combination with the more widely investigated photo-electro-chemical (PEC) water splitting to combine vibration and solar harvesting. To overcome the challenges of photo-electro-chemical water splitting, such as the limited absorption of visible light, Tan *et al.* fabricated a piezoelectric-photo-electro-chemical hybrid device that combined harvesting from both light and vibration using piezoelectric ZnO nanorods on one-dimensional nanowire conductors. This multiple-energy-source powered system was based on a metal–semiconductor branched hetero-structure of Ag/Ag_2S–ZnO/ZnS that was partially encapsulated with PDMS for piezoelectric harvesting, while the exposed part acted as a catalyst to enhance the photo-electro-chemical performance of the ZnO nanorods. The system was initially characterised separately under UV-vis irradiation and under ultrasonic vibrations, as in Fig. 14a.[55] Under simultaneous application of UV-vis light and vibration, as in Fig. 14b, the generation of piezoelectric charge and charge transfer between the active electrode and Pt electrode generated a voltage bias, as in Fig. 14b, which improved the photocurrent density from 8 mA m^{-2} (no vibration) to 22 mA m^{-2} (with vibration). The system was also used to enhance photo-electric-chemical degradation of methyl orange for water treatment. Yang *et al.* have utilised the polarisation of piezoelectric $BaTiO_3$ to enhance photo-electro-chemical (PEC) water splitting.[56] An enhanced performance of PEC photo-anodes was reported due to ferroelectric polarisation-enhanced band engineering of $TiO_2/BaTiO_3$ core/shell nanowires.

3.2 Piezo-electro-catalytic degradation of organic pollutants

In addition to harvesting mechanical vibration for water splitting, the piezoelectric effect has been used for degradation of organics in water. After exploiting the piezoelectric effect for water splitting, Hong *et al.* explored a similar approach for Azo Dye decolourisation in aqueous solutions[57] and for the degradation of Acid Orange 7 (AO7), the origins of the electron–hole pairs were from strained piezoelectric $BaTiO_3$ micro-dendrites. By harvesting ultrasonic vibrations the AO7 dye was degraded by nearly 80% after subjecting the material to 90 min of vibration. Using the same mechanism, Lin *et al.* used the piezoelectric properties of $Pb(Zr_{0.52}Ti_{0.48})O_3$ (PZT) fibres to harvest mechanical vibrations and further improve efficiency due to the large amount of electrical charge generated by the highly piezo-active PZT material.[58] In 2017, Lv *et al.* focused their work on investigating the piezo-electro-chemical effect to degrade AO7 using $BaTiO_3$ in the presence of metal ions, since calcium, magnesium, aluminium, iron and copper are frequently found in waste water.[59] The fundamentals of the piezo-photo-chemical mechanism have been described by Z. L. Wang.[60] When the piezoelectric is subjected to a periodically applied strain during vibration the photo-generated electrons and holes migrate to the surface in opposite directions under the influence of the electric field

produced by the piezoelectric effect; thereby achieving a higher efficiency due to suppression of electron–hole recombination.

Xue *et al.* used ZnO nanowires that combine the properties of a piezoelectric and a semiconductor. The photo-catalytic activity of ZnO nanowires was enhanced by the piezoelectric and electric field driven separation of the photo-generated carriers for the degradation of methylene blue (MB).[61] The working mechanism for the piezo-photo-catalytic activity of ZnO nanowires in the work of Xue *et al.* is shown in Fig. 15 where Fig. 15a shows the woven ZnO nanowires/carbon fibres (CFs) without an applied force or UV irradiation. When subjected to UV light, as in Fig. 15b, there is a transition of electrons from the valence band to the conduction band, leaving an equal number of holes. When a periodic force is simultaneously applied to the ZnO nanowires/CFs, as in Fig. 15c, there is a relative motion between neighbouring ZnO nanowires that results in bending of the ZnO nanowires which produces positive and negative piezoelectric potentials across their width. The generated piezoelectric field then drives electrons and holes to migrate to the surface in opposite directions and the recombination of electrons and holes is therefore reduced. The electrons (e^-) react with dissolved oxygen molecules to yield superoxide radical anions ($^{\bullet}O^{2-}$), and the holes (h^+) are ultimately trapped by H_2O at the surface to yield $^{\bullet}OH^-$ radicals, Fig. 15d. The hydroxyl radicals can oxidize MB in aqueous solution, generating non-toxic CO_2 and H_2O. The photo-catalytic efficiency of ZnO nanowires was thought to be enhanced by the piezoelectric field and reduced recombination of photo-generated carriers.

To exploit the same combination of piezoelectric and semiconducting properties, Lo *et al.* used $ZnSnO_3$[62] and Wang *et al.* used $Zn_{1-x}SnO_3$.[63] Fig. 16 shows the increased rate of degradation of methylene blue by applying both stress and UV on

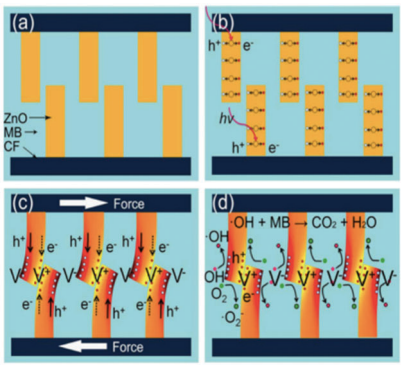

Fig. 15 Mechanism for piezo-photo-catalytic activity of ZnO nanowires. (a) ZnO nanowires/carbon fibres (CFs) without an applied force or UV irradiation. (b) UV illumination of ZnO leads to transition of electrons from the valence band to the conduction band, and equal number of holes. (c) When a force is applied, bending of ZnO produces positive and negative piezoelectric potentials across their width. The piezoelectric field drives electrons and holes to the surface in opposite directions. (d) Electrons (e^-) react with dissolved oxygen molecules to yield superoxide radical anions ($^{\bullet}O_2^-$) and holes (h^+) are trapped by H_2O at the surface to yield $^{\bullet}OH^-$ radicals. The hydroxyl radicals oxidize methylene blue (MB) in aqueous solution. Reprinted from ref. 61, Copyright (2015), with permission from Elsevier.

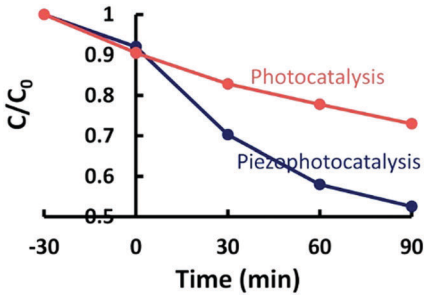

Fig. 16 Self-photo-degradation of methylene blue (MB) and photo-catalytic activity of piezoelectric $ZnSnO_3$ nanowires with and without applied stresses and UV irradiation. Reprinted with permission from ref. 62. Copyright (2015) American Chemical Society.

piezoelectric $ZnSnO_3$ nanowires; see the blue piezo-photo-catalysis curve.[62]

To further improve the piezo-photo-catalytic effect Hong *et al.* used CuS/ZnO hetero-structure nanowire arrays that were subjected to a combination of UV and ultrasonic irradiation to degrade MB.[64] Sun *et al.* used Ag_2O/ZnO nano-tetrapods, Zhang *et al.* used Ag/ZnO and Li *et al.* used $Ag_2O/BaTiO_3$.[38,65,66] Again, the higher efficiency and speed of degradation was attributed to the coupling between the built-in electric field of the hetero-structure and the piezoelectric field of ZnO under strain that enhanced electron–hole separation and migration in opposite directions. This is demonstrated in Fig. 17, where the ZnO that is on a stainless steel mesh is mechanically deformed due to the application of ultrasound and this leads to an electric field across the wire. Since the wire is also photo-excited by solar radiation, electrons and holes are separated due to the applied field towards opposite directions and drive the surface reactions, Fig. 17(a). Fig. 17(b) shows the effect that the field has on the energy bands that separate the photo-excited electrons and holes in opposite directions.

Further information on the influence of ferroelectricity and piezoelectricity on photo-catalytic activity and surface chemistry, in the absence of vibration, can be found in a recent review[67] and a number of key papers by Dunn *et al.*[68–74] Since ferroelectric materials are both piezoelectric and pyroelectric there is significant scope for further efforts to harvest thermal and mechanical energy in combination with light for enhancing electro-chemical reactions.

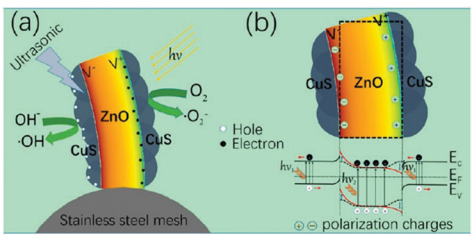

Fig. 17 (a) Schematic of piezo-photo-catalytic process of CuS/ZnO nanowires on stainless steel mesh under combined solar and ultrasonic irradiation. (b) Schematic of energy band diagram of CuS/ZnO hetero-structure under both solar and ultrasonic irradiation. Reprinted with permission from ref. 64. Copyright (2016) American Chemical Society.

3.3 Piezo-electro-chemical self-charging of power cells

Energy generation and energy storage are two distinct processes and are usually accomplished separately. However, in 2012 Xue *et al.* introduced a new mechanism where harvested mechanical energy was directly stored as chemical energy.[75] The polyethylene separator of a conventional lithium battery was replaced with a piezoelectric PVDF polymer. When the device was subjected to a compressive strain, the piezoelectric induced electric field of the PVDF separator acted to drive electrical charges from the cathode to the anode, thereby charging the power cell. Later, the same group fabricated a novel integrated self-charging power cell (SCPC) that combined a CuO anode with a PVDF separator in the form of CuO/PVDF nano-arrays. The high efficiency of the cell was attributed to the intimate contact and large interface area between the anode and separator.[76] This is shown in Fig. 18 and when a compressive stress is applied, the PVDF creates a positive piezo-potential at the cathode and a negative piezo-potential at the anode (Fig. 18(b)). Lithium ions then migrate in the electrolyte from the cathode to anode under the generated electric field, leading to charging reactions at the electrodes (Fig. 18(c)) until chemical equilibrium of the two electrodes is re-established and the self-charging process ceases. When the compressive stress is released, the piezoelectric field of the PVDF disappears, which breaks the electrostatic equilibrium, and residual lithium ions diffuse back to the cathode; see Fig. 18(c). In such a system rectification is not required since it is operated in compression only, so that the polarity of the system is maintained; although care would need to be taken to ensure tensile loads are not experienced by the system.

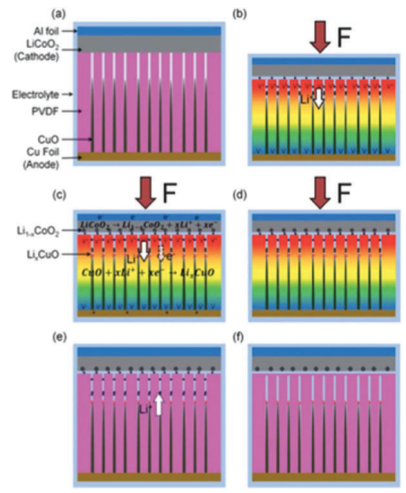

Fig. 18 (a) Schematic of self-charging power cell in discharged state. (b) Under a compressive stress the piezoelectric PVDF creates a piezo-potential with a positive potential at the cathode and a negative piezo-potential at the anode. (c) Under the internal piezoelectric field, lithium ions migrate in the electrolyte from cathode to anode, leading to charging reactions at the electrodes. (d) Chemical equilibrium of the two electrodes is re-established and self-charging ceases. (e) When the compressive force is released, the piezoelectric field disappears, which breaks the electrostatic equilibrium and residual lithium ions diffuse back to the cathode. (f) The electro-chemical system reaches a new equilibrium, and self-charging is complete. Reproduced from ref. 76 with permission of The Royal Society of Chemistry.

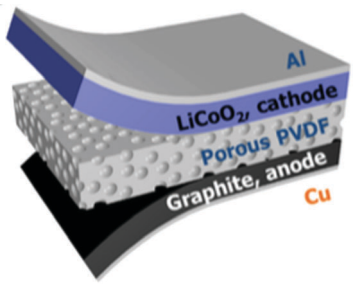

Fig. 19 Schematic diagram of a self-charging power cell (SCPC) consisting of $LiCoO_2$ as the cathode, artificial graphite as the anode, and a porous PVDF piezo-separator. Reproduced from ref. 77 with permission of The Royal Society of Chemistry.

Approaches to further improve the energy conversion and storage efficiency include the use of a composite or porous separator. Xing *et al.* used a mesoporous PVDF separator that lowered the charge transfer resistance.[78] Highly porous PVDF, PVDF–PZT nano-composites and PVDF–ZnO composites have also been examined.[77,79,80] Fig. 19 shows a typical device architecture with a porous PVDF separator, graphite anode, and $LiCoO_2$ cathode.

It is desirable to improve the integration level and minimise energy loss in the power-management circuits between energy harvesting and storage devices. Song *et al.*, Ramadoss *et al.*, and Wang *et al.* integrated a piezoelectric separator in a supercapacitor[80–82] and to further improve the performance Parida *et al.* used a poly(vinylidene fluoride)-trifluoroethylene (P(VDF-TrFE)) foam as a piezoelectric separator and designed a double layer capacitor with fast absorption and desorption of ions at the carbon nanotube electrodes.[83] A different approach to use the piezoelectric effect for enhanced charge storage was proposed by Lee *et al.* The mechanical stress from the expansion of silicon during lithiation was transferred *via* a conductive carbon nanotube (CNT) based matrix to ferroelectric $BaTiO_3$ particles so that a piezoelectric potential was generated.[84] This is shown in Fig. 20, where the silicon and $BaTiO_3$ particles are dispersed in a CNT matrix (Fig. 20(a)). Lithiation of the silicon nanoparticles results in a volume increase that applies pressure to the $BaTiO_3$ nanoparticles to create a piezoelectric potential (Fig. 20(b)) that enhances the mobility of the lithium ions in the subsequent discharging and charging processes.

A particularly novel approach by Kim *et al.* does not use the piezoelectric effect, but is based on stress driven electrochemical effects.[85] In this design different stress states are induced by bending partially lithium-alloyed silicon electrodes which creates a potential difference between the electrodes. Fig. 21 shows the working mechanism. In the initial stress-free condition, the two electrodes are at an iso-potential (Fig. 21(I)). Bending of the device generates tension in the lower electrode and compression in the upper electrode in Fig. 21(II). The asymmetric stress state creates a chemical potential difference

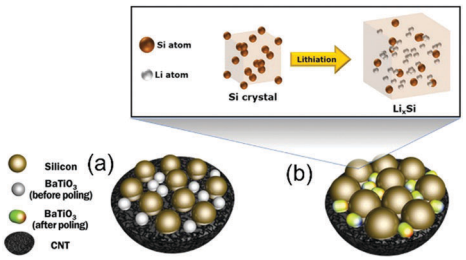

Fig. 20 Schematic of microstructural changes in the Si/carbon nanotube(CNT)/$BaTiO_3$ nanocomposite anode during lithiation. (a) Si and $BaTiO_3$ particles are dispersed and attached to the CNT. (b) Lithiation of Si results in a large increase in volume, pressurising $BaTiO_3$ nanoparticles to create a piezoelectric potential. Adapted with permission from ref. 84. Copyright (2016) American Chemical Society.

that drives Li^+ migration from the compressive electrode to the tensile electrode through the electrolyte (Fig. 21(III)). In order to maintain charge neutrality, electrons flow in the outer circuit from the compressive and to the tensile electrodes, thereby generating electrical power. The Li^+ migration continues until the potential difference vanishes, and a new equilibrium state on the two electrodes with different lithium concentrations are achieved (Fig. 21(IV)). When the external stress is removed by unbending the device, the chemical potential shifts on the electrodes and the difference in lithium concentration between the electrodes drives Li^+ migration in the opposite direction (Fig. 21, back to I), thereby discharging the device. This provides an interesting approach to harvest mechanical motion for electro-chemical based energy generation, which could be enhanced by coupling to piezoelectric effects to generate an additional electric field to enhance ion migration.

3.4 Other piezo-electro-chemical applications

Noris-Suarez have reported bone healing due to piezoelectricity.[86] Bone healing and growth are controlled by the rate of deposition of hydroxyapatite (HA) and their work showed that the piezoelectric dipoles produced by deformed collagen can produce the necessary precipitation of HA. Therefore there is scope to harvest bio-mechanical motion for enhanced bone growth. Lang *et al.*[87] demonstrated that HA is both piezoelectric and pyroelectric indicating potential for harvesting human motion and temperature changes; the reader is referred to a review on the topic by Baxter *et al.*[88] A biomimetic approach was used by Soroushian *et al.* who investigated self-healing structures that were able redistribute their structural mass in response to dynamic loads.[89] In their work the piezoelectric effect was used to convert dynamic mechanical energy applied to a structure into electrical energy that was able to drive an electro-chemical self-healing phenomena within a solid electrolyte. Zhang *et al.* also used PVDF to use piezoelectric energy to indirectly power cathodic protection[38] and the output of the fabricated device was used to protect metal surfaces from the chemical corrosion, see Fig. 9. Touach *et al.*[90] used lithium niobate ($LiNbO_3$) as a ferroelectric and photo-catalyst material as a cathode catalyst for wastewater-fed single-chamber microbial fuel cells (MFCs); microbial cells are also discussed with regard to thermo-electrics (Section 6).

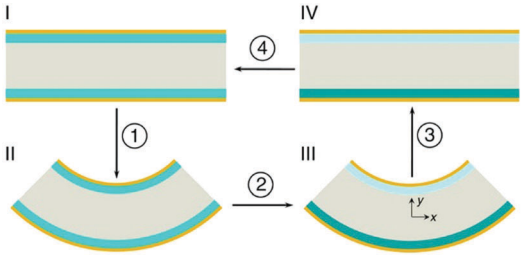

Fig. 21 Schematic of the cross-section of the device in operation using partially lithium-alloyed silicon electrodes. Reproduced from Kim *et al.*[85] with permission from Nature Publishing Group (Copyright 2016).

4. Tribo-electro-chemical effects

Compared with the piezo- and pyro-electric based energy harvesters, the utilisation of the triboelectric effect in a tribo-electric nanogenerator (TENG) to scavenge mechanical energy is a relatively new approach in the field of energy harvesting, and was first reported in 2012 by Z. L. Wang's group.[91] The mechanism of charge generation exploits the intrinsic ability of materials in different positions of the triboelectric series to gain or lose charge when they make contact with each other. The triboelectric charges that are generated on the surface of the two materials can be regarded as a combination of tribo-electrification and electrostatic induction. TENGs typically have four basic working modes, which are shown in Fig. 22.[8] The generation of charge relies on contact and separation cycles between two different materials and the modes of operation can involve rubbing or contact between two materials under vertical (Fig. 22a) or lateral sliding (Fig. 22b), with two electrodes to collect the charge. Single-electrode configurations can also be

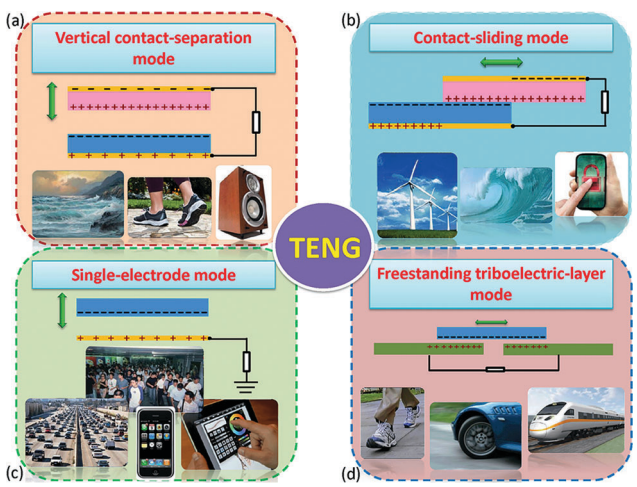

Fig. 22 The four working modes of the triboelectric nanogenerators (TENGs). (a) vertical contact-separation mode, (b) lateral-sliding mode, (c) single-electrode mode, and (D) freestanding triboelectric-layer mode. Reproduced from ref. 8. with permission from The Royal Society of Chemistry.

employed, as seen in Fig. 22c, and freestanding moving objects without an electric connection can be utilised; see Fig. 22d. In all of the potential modes of operation, the movement of the free electrons enables the generation of a current that flows in an external circuit, which can be an electro-chemical system, storage capacitor or an electrical load.

TENG devices are being rapidly developed with increasing efficiency in terms of their ability to convert mechanical energy into electricity. The power densities and instantaneous energy conversion efficiency for a single device has been reported to be as high as 500 W m^{-2} and 70%.[92,93] Owing to their high power density, high efficiency, small volume, light-weight nature and low fabrication cost, TENGs are attracting potential in harvesting 'blue energy' from wave power.[94]

The energy that is harvested from ambient environments by TENGs varies significantly and can be periodic, random and time-dependent, which results in an alternating current (AC). Moreover, the magnitude of the pulsed voltage in TENGs is relatively high (typically 2 V to 1.3 kV, see Table 1) while the current remains relatively low (85 nA to 13 mA, see Table 1) which often requires the use of a power management circuit. As a result, when TENGs are coupled to electro-chemical processes, they can act as the power source either by directly powering the electro-chemical system with a pulsed output that is rectified to maintain the polarity of the output or a combination of transformer (to step down the voltage) and rectifier that is used to charge an integrated capacitor/battery before supplying the electro-chemical system with a direct current (DC) electrical output. As a result, integrated TENG-controlled electro-chemical systems often consist of a triboelectric generator, an AC/unipolar signal converter with a rectifier and/or transformer and the functional electro-chemical unit. Cao *et al.* have provided an excellent review on triboelectric nano-generators and electro-chemical systems.[95] Here we will concentrate on the introduction to the mechanisms of tribo-electric generation for controlling electro-chemical processes and describe recent achievements in electro-chemical processes controlled by TENGs.

4.1 Tribo-electro-chemical water splitting

As discussed in Section 2.1, water splitting can be electrically triggered when the potential difference between the anode and cathode is greater than 1.23 V (eqn (1) and (2)). Triboelectric nanogenerators have been used to harvest ambient sources of mechanical energy and supply electrical power to achieve electro-chemical water splitting without the need for an external power source.[96–98] Yu *et al.*[99] fabricated a wind-driven TENG to supply a bias voltage after rectification between a platinum counter electrode and a working electrode with a 3-D structure based on TiO_2 nanowires and graphite fibres. The combined system provided enhanced photo-catalytic activity and generated 4.87 mmol (h g)$^{-1}$ H_2 with the aid of solar illumination and wind, this was almost three times higher than a TiO_2@MoS_2 catalyst under a visible light source.[100] Fig. 23(a) shows the system with the wind powered TENG, and rectification bridge to maintain electron flow in one direction. Under the application of wind and

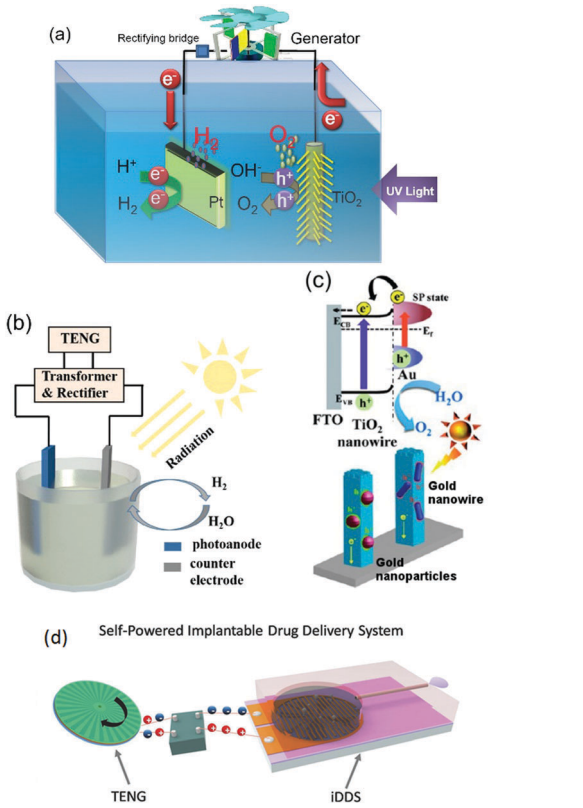

Fig. 23 (a) Schematic of photo-electro-chemical water decomposition with bias voltage from a TENG. Reprinted from ref. 99. Copyright (2015) with permission from Elsevier. (b) Schematic of the TENG-photo-electro-chemical (PEC) hybrid cell. Reproduced with permission from ref. 101. Copyright 2017, John Wiley and Sons. (c) Charge transfer schematic of Au–TiO_2 used in the TENG-PEC hybrid cell. Adapted with permission from ref. 102. Copyright (2013) American Chemical Society. (d) Schematic of the TENG-based implantable drug delivery system (iDDS). With permission from ref. 103. Copyright 2017, John Wiley and Sons.

UV light, hydrogen generation was observed on the counter electrode. However, due to the relatively low current density on the TiO_2 nanowire/graphite fibre electrode and the resistance mismatch between the TENG, electrical load and electrochemical system, Li *et al.*[101] combined both electrolysis and photo-electro-chemical (PEC) effects to improve H_2 production and increase solar efficiency. Fig. 23(b) shows the system employed, that used a TENG driven by a linear motor to supply a potential across a photo-anode and counter electrode. A lithium-ion battery, not shown in Fig. 23(b), was used to provide a stable DC output (1.5 V) after being charged by a TENG for 42 min using rectification and transformation, where a series of loads of different resistance were chosen to match the electrical impedance in the external circuit. A similar photo-anode approach was used by Pu *et al.* to achieve enhanced photo-activity by a surface plasmonic resonant effect.[102] This anode consisted of Au nanoparticle decorated TiO_2 arrays on fluorine doped in tin oxide (FTO) conductive glass, as shown in Fig. 23(c). Au nanoparticles were used to localize the optical energy due to the surface plasmonic resonance and the interaction between this electric-field amplification and TiO_2 promoted photon absorption. In addition, the gold nanoparticles

also act as a photosensitiser when the wavelength of the surface plasmonic resonant matches the optical band gap of TiO_2, therefore hot electron injection from Au to the TiO_2 conduction band was enhanced under visible light.[102] This coupled TENG-photo-electro-chemical (PEC) hybrid cell provided a route to split water by converting mechanical and solar energy into chemical energy. Interestingly, the generated H_2 and O_2 on the anode and cathode from water splitting has also been employed to pressurise a drug solution in a reservoir for an implantable drug-delivery system (iDDS);[103] see Fig. 23(d) which shows the TENG, rectification, and the implantable drug delivery system. Yang *et al.*[97] developed a hybrid energy cell that integrated a TENG, a thermoelectric cell and a solar cell that could simultaneously harvest mechanical, thermal and/or solar energies for water splitting; the specific application of thermo-electrics to electro-chemical systems will be described in more detail (Section 6).

4.2 Tribo-electro-chemical degradation and wastewater treatment

The pyroelectric effect, which harvests temperature fluctuations, and the piezoelectric effect, that harvests vibrations, has been used for water treatment, as discussed in Sections 2.1.2 and 3.2 respectively. TENGs that harvest motion have also attracted interest as a form of self-powered electro-chemical wastewater treatment and SO_2 removal as it is environmentally friendly and does not create toxic waste.[37,104–109] Zheng *et al.*[110] deployed a TENG to remove toxic organics in water; this included aniline (ANI) and $N(p\text{-}C_6H_4Br)_3$ which was removed *via* an oxidation process; the performance of the self-powered treatment by a TENG was reported to be as effective as an electro-chemical workstation which requires a galvanostat as an external power source. Gao *et al.* fabricated a TENGs with either a multilayer-linkage configuration (rd-TENG in Fig. 24(a)[111] or a rotary disc-structure[112] which were used as a self-powered unit to drive a water treatment process). In both cases rectification of the TENG output was used to ensure a unipolar supply to the anode and cathode along with a transformer to reduce the operating voltage as the potential produced by a TENG is typically higher than other harvesting systems, see Table 1. The TENGs were used for the removal of highly toxic and carcinogenic organics by conversion to CO_2; this included oligomers, azobenzene dye and 4-aminoazobenzene. The electric oxidation potentials were controlled *via* either the resistance of the external load or the numbers of the friction layers in the TENG device. In later work, the metal electrode was replaced with a carbon material manufactured from bean curd that was used to degrade methyl red.[113]

In addition to the above toxic chemical compounds, heavy metal ions (such as Cu, Ni and Cr) are another main component in wastewater, which can cause severe illness when they enter our food chain. One of the most promising ways for reducing heavy metal ions is electro-deposition where the heavy metal can be reduced and collected from the surface of the electrode.[114] Chen *et al.*[115] employed a TENG as a power source connected to a sewage treatment system, shown in the left of

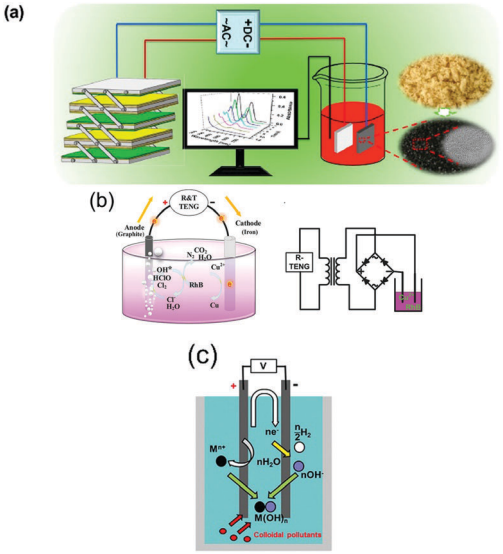

Fig. 24 (a) Schematic of the multi-layer TENG driving electro-chemical degradation. Reprinted with permission from ref. 113. Copyright (2017) American Chemical Society. (b) (left) Schematic diagram of the Cu^{2+} and Rhodamine removing powered by TENG and (right) the corresponding circuit diagram of this self-powered electro-chemical recovery system. Reproduced with permission from ref. 115. Copyright 2016, John Wiley and Sons. (c) Operation of the electro-coagulation process. Reprinted from ref. 117. Copyright (2016) with permission from Elsevier.

the Fig. 24(b). Using a NaCl solution as the electrolyte, toxic Rhodamine B was degraded into CO_2, H_2O, and N_2 at the anode, while the heavy metal copper ions were electrodeposited at the cathode, see right of the Fig. 24(b). It was demonstrated that the removal efficiency of Rhodamine B and Cu^{2+} from a pulsed electrical output from a TENG harvester was better than that of a DC supply. Similar research on Cu^{2+} reduction was also reported by Yeh *et al.*[116] who used a TENG operating in a freestanding mode (Fig. 22(d)) which was coupled to the anode and cathode to drive the electro-chemical reduction of Cu^{2+} ions on the surface of the cathode in an aqueous based solution. Other wastewater electro-chemical treatments, such as electro-coagulation, can be driven by TENGs as demonstrated by Jeon *et al.*[117] In this case, wind energy was utilised to generate electrical power *via* a TENG to power an electro-coagulation unit. In their system, shown in Fig. 24(c), metal ions (M^{n+}, which are Al^{3+} in the work) were generated at the anode while OH^- ions were generated at the cathode. Colloidal pollutants, such as algae and dyes, reacted with the insoluble metal hydroxide and produce flocs which form coagulated pollutants so that clean water could be collected from the top of the water treatment system.

Li *et al.*[118] recently built an electro-chemical ramie fiber degumming system and wastewater treatment with a water-driven TENG. Raw ramie fibers are a common textile material and exist as fiber bundles where the individual fibers are bonded to each other In order to extract the individual cellulose fibers the harvesting system shown in Fig. 25(a) was constructed; the system consisted of (i) a TENG, power management (transformer/rectification circuit and capacitors) and reaction pond, (ii) a Ti/PbO_2

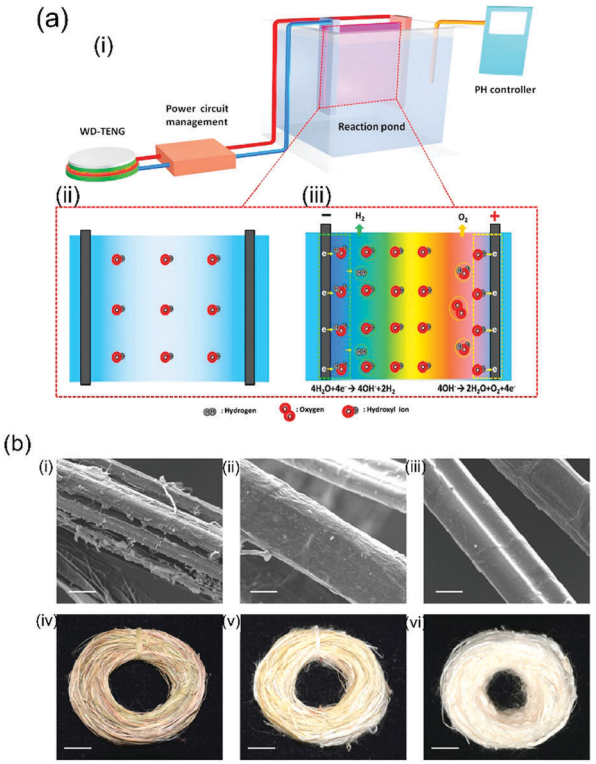

Fig. 25 (a) Working principle of the triboelectric ramie fibre degumming and self-powered wastewater treatment, (b) SEM images of (i) raw ramie fibers and (ii) degummed ramie fibers without TENG and (iii) degummed ramie fibers with TENG. Scale bars are 20 μm. Photographs of (iv) raw ramie fiber and (v) degummed ramie fiber without TENG and (vi) degummed ramie fiber with TENG. Scale bars are 1.5 cm. Reprinted from ref. 118. Copyright (2016) with permission from Elsevier.

anode and titanium cathode immersed in the reaction pond. Due to the potential difference produced by TENG, hydroxyl ions move towards the anode which make the gummy materials break away from the cellulose part of the fiber which are then readily dissolved in a hot alkaline solution; see Fig. 25(a, iii). The surface of the treated fiber with the TENG exhibited the most clean and smooth surface, as shown in (c) and (f) in Fig. 25(b). Furthermore, the degumming wastewater was also electrochemically degraded using a TENG after finishing the fiber treatment.

4.3 Tribo-electro-chemical corrosion protection

Cathodic protection is a common technique for protecting metals from corrosion to increase service life of metallic components and reducing maintenance costs; this can be achieved by applying organic coatings or using an electrochemical cell. In a typical electro-chemical protection procedure, the metal to be protected will have an ohmic-contact to the negative polarity of the external power source and an inert electrode will be connected to the positive pole. Both electrodes are then placed in the corrosion electrolyte to form an electrolytic cell so that the metal will be protected as the cathode. Inspired by preliminary work[119–123] on the realisation of cathodic protection powered by TENG, recent efforts have been undertaken

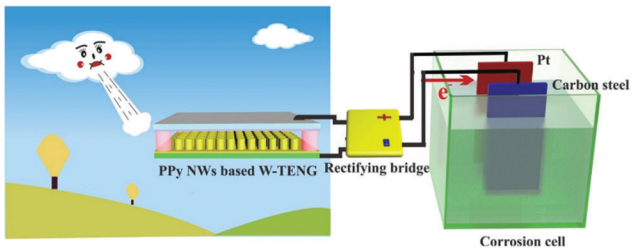

Fig. 26 Device structure of the cathodic protection system powered by polypyrrole nanowire (PPy NW) based TENG driven by wind (W-TENG). Ref. 125 – published by permission of The Royal Society of Chemistry.

on optimising the triboelectric material,[124] using a conductive polymer PPy (polypyrrole)[125] or combining TENGs with the piezo- and pyro-electric effects to form hybrid systems[38] to ensure the cathode is below the corrosion potential to prevent corrosion. Fig. 26 shows an example of wind driven TENG whose output is rectified and then connected to platinum counter electrode and carbon steel for cathodic protection.[125] In addition, the triboelectric effect has also been adopted for anti-fouling applications, where the pulsed energy generated by a TENG is used to remove or prevent the accumulation and growth of organisms on both anode and cathode, as demonstrated by Feng *et al.*[124]

4.4 Tribo-electro-chemical synthesis (electro-deposition and electro-oxidation)

Energy harvesting by TENGs has also been used for materials processing. Electro-deposition is a process that uses an electrical current to reduce cations of a desired material from a solution and coat the material as a thin film onto a conductive substrate surface. TENGs have been used by Zhu *et al.* to harvest ambient mechanical energy for a self-powered electrodeposition process.[126] Due to the risk of oxidation or corrosion of the metallic TENG electrodes when exposed to a wet environment, a conducting polymer polypyrrole (PPy) was chosen as the electrode to fabricate an all-plastic based TENG that included an integrated PPy-based supercapacitor, thereby providing sustainable power.[127] Wang[128] has recently exploited TENGs to provide a pulsed rectified output to electrochemically polymerise PPy for up to nine chemical reactors; see Fig. 27. Similarly, TENGs can also facilitate the oxidation process for preparation of mesoporous Al_2O_3.[129] A cross-linked TENG was designed by Zheng *et al.*[110] which could supply power to chemically synthesise polyaniline (PANI) *via* either oxidisation of PANI-OH or ANI in an H_2SO_4 aqueous solution.

4.5 Additional tribo-electro-chemical applications

Additional electro-chemical research based on the triboelectric effect has been undertaken in the application of the electrochemical sensing[107,130–135] and electro-chromic applications.[136–142] Due to the different triboelectric polarity between Hg^{2+} and Au nanoparticles (Au NPs), Hg^{2+} can selectively bond to the surface of the Au NPs. Lin *et al.*[132] exploited this effect to detect and measure the concentration of Hg^{2+} using a self-powered

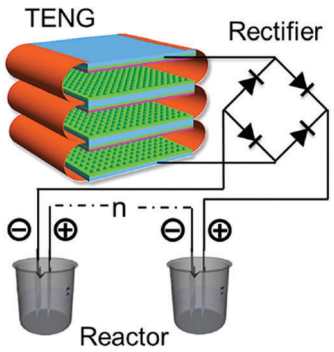

Fig. 27 Schematic of the self-powered synthesis and reactor system. Reproduced with permission from ref. 128. Copyright 2016, John Wiley and Sons.

triboelectric nano-sensor. TENG powered electro-chemical sensors have been reported that could detect humidity,[143] melamine[144] and ultraviolet light.[145,146] Furthermore, electrochromic materials were able to interact with the electrical energy produced by a TENG to achieve a colour change or to fluoresce continuously and reversibly during electrochemical oxidation and reduction. A number of research efforts[136,139–141,147] have shown that TENGs can supply a sufficient electrical output to stimulate electro-chromic behaviour either in a cathode (colour change under a negative potential) or anode (colour change under a positive potential).

5. Flexo-electric and electro-chemical effects

While the piezoelectric effect relates to the generation of charge in response to an applied strain, the flexoelectric effect involves the generation of charge due to the presence of a strain-gradient. Biomembranes exhibit flexoelectric effects and are the basic building units of many cells and cellular structures.[148] The phospholipid molecules in most biomembranes are organised in a bilayer format, as shown in Fig. 28, and both artificial and natural cell membranes have been shown to exhibit direct flexoelectricity (current generation from curvature) and converse flexoelectricity (voltage-induced curvature changes).[149–151] Phospholipid molecules include a hydrophilic phosphate head and a hydrophobic C–H chain, as shown in Fig. 28(a),[152] which resembles a cone and has a dipole directed toward the apex. Under the application of electric field the bilayer membrane that has proteins with an intrinsic polarisation, p_p, undergoes a splay deformation *via* the converse flexoelectric effect.

Direct flexoelectricity in biomembranes results from a curvature-induced polarisation of the liquid crystal membrane, in which the molecules (lipids, proteins) of the membrane are initially uniaxially orientated as shown in Fig. 28(b).[153] In this flat bilayer membrane, the polarised cones are randomly directed, with no net polarisation. However, when subjected to bending, as in Fig. 28(c),[153] a conformational change occurs that imposes a polar symmetry, so that on one side of the membrane the

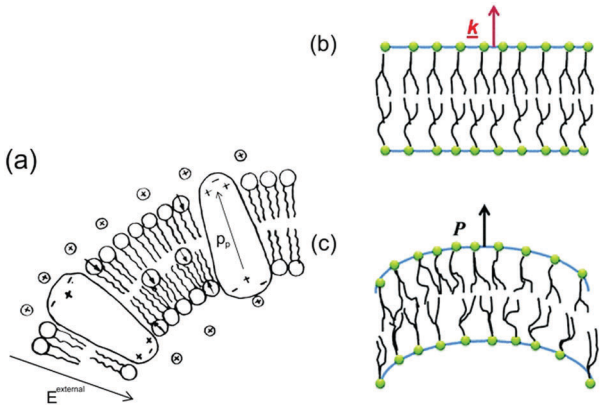

Fig. 28 Flexo-electricity in biological membranes. (a) Schematic of bilayer lipid membrane under external electrical field, and globular proteins with an intrinsic polarisation. Ref. 152 – Copyright 1975, with permission of Springer. (b) Under planar conditions there is no polarisation and (c) Under bending the lower surface is in compression and the upper one in dilation, and an electric polarisation is generated. Reprinted figure with permission from ref. 153 Copyright (2013) by the American Physical Society.

molecules move apart whereas on the other side they move closer together.[154,155] The resulting polarisation (P) is:

$$P = f \cdot k \cdot n \quad (6)$$

where f is the flexoelectric coefficient, k is the mean curvature and n is the normal vector to the membrane. Petrov discussed experimental evidence of flexoelectric phenomenon[148,155–157] and Ahmadpoor *et al.* has presented a thorough review on soft biological membranes.[158]

Flexoelectricity has been found to have implications for mechano-sensitivity and mechano-transduction in living systems, including ion transport[155,159] and the hearing mechanism in mammals.[160–163] Petrov *et al.*[159] proposed a model for ion transport in biological systems, as shown in Fig. 29, which demonstrates an ion pumping through a membrane. The driving force for ion transport is a flexoelectric electric field from a change in curvature of the bilayer membrane induced by Adenosine triphosphate (ATP) and ionic concentration gradients. The resulting curvature induces polarisation and creates a depolarising electric field that acts as a driving force for ion pumping. Similar flexoelectric effects are responsible

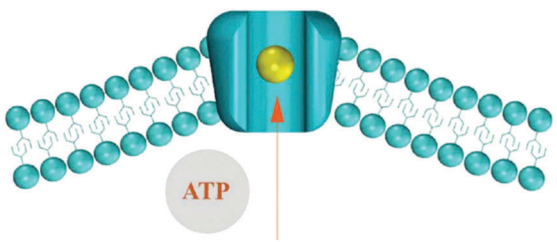

Fig. 29 Ion pump model proposed by Petrov. The presence of ATP and ions lead to curvature of the phospholipid bilayer. This results in a flexo-electric polarisation and the electric field produced is the driving force for ion pumping. Membrane, ion and adenosine triphosphate (ATP) shown. Ref. 158 Reproduced by permission of The Royal Society of Chemistry.

for the main transduction component for sensing sound in mammals as inner hair cells consist of flexoelectric stereocilia that transform mechanical vibrations into electrical potentials that are sensed by the nervous system.[160–163] The ability of biological membranes and cells to exhibit flexoelectric effects to achieve ion pumping and sensing could inspire new methods to harvest mechanical motion to drive ions in electro-chemical systems at the nano-scale.

5.1 Flexo-electric energy harvesting

The potential of flexoelectricity in energy harvesting has been examined by several researchers. Significant enhancement of the piezoelectric coefficient of a piezoelectric nano-beam/ribbon due to flexoelectric effect has been reported.[164,165] Pre-stretched buckled PZT ribbons show high strain gradients that provides charge in addition to the conventional piezoelectric effect.[165]

Majdoub *et al.* used a continuum model to show that flexoelectricity can lead to an enhancement of electromechanical coupling of non-uniformly strained piezoelectric and non- piezoelectric nanostructures.[164] For example, $BaTiO_3$ nanobeams with a thickness of 5 nm experienced inhomogeneous strains almost five times larger than macro-scale $BaTiO_3$ beams. Therefore in a narrow range of geometric dimensions, piezoelectric nanostructures can exhibit dramatically enhanced energy harvesting capability due to flexoelectric effects. For a PZT cantilever beam, the total harvested power increased by 100% for a 21 nm beam thickness under short circuit conditions and ~200% increase could be achieved for tailored cross-sections.[166] Deng *et al.* developed a continuum model for flexoelectric nano-scale energy harvesting for cantilever beams, as shown in Fig. 30(a) where the polarisation due to the resulting strain gradient is shown in Fig. 30(b). On bending an AC potential difference is generated across the electrodes on its upper and lower surfaces. The output power density and conversion efficiency increased significantly when the beam thickness was reduced from the micro- to nano-scale and conversion efficiency at sub-micron thickness levels increases by two orders of magnitude as the thickness was reduced by an order of magnitude. Wang *et al.*[167,168] has also presented analytical model for nano-scale energy harvesters using flexoelectric effects.

Han *et al.* have reported a flexoelectric nanogenerator consisting of direct-grown piezoelectrics on multi-walled carbon nanotubes (mwCNT) in a PDMS matrix.[169] Nano-generators based on lead zirconate titanate (PZT)-mwCNTs generated a voltage of 8.6 V and a current of 47 nA from a mechanical load of 20 N; see Table 1. The high performance was reported to originate from the strong connection between the PZT and mwCNTs with an enhanced flexoelectric effect due to the strain gradient in the material. The epitaxial PZT nanogenerators with an internal strain distribution are shown in Fig. 31 where the change in lattice spacing indicates a strain gradient, which are thought to contribute to the enhancement of the nanogenerator properties of the PZT-nwCNT films by combining both flexoelectric and piezoelectric effects. This provides scope for improving the charge generation capability of some of the piezoelectric materials discussed above, in particular nano-sized materials and generators. Rey *et al.* developed a bio-inspired mechanical energy harvester consisting of a soft flexoelectric membrane[148] subjected to fluid-flow-generated mechanical oscillations.[153] Deformable flexoelectric membranes were used as the basic unit of transduction, as in Fig. 28, where bending of the membrane leads to an electric polarisation or an electric field leads to bending. This is shown in Fig. 32 where the open circuit (displacement, $D = 0$) and closed circuit (electric field, $E = 0$) states are shown and bending is imposed by an externally imposed pressure drop from the contacting fluid phases (P_1 and P_2) and charge separation in the membrane is due to the flexoelectric effect.

Flexoelectric materials can therefore provide new approaches to create nanodevices for sensing and electromechanical energy

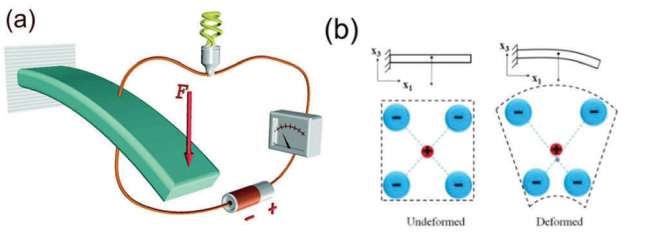

Fig. 30 (a) Schematic of a centro-symmetric flexoelectric energy harvester under base excitation. Ref. 158 – reproduced by permission of The Royal Society of Chemistry. (b) Polarisation due to bending of a centro-symmetric beam. Reprinted from ref. 170, with permission from Elsevier.

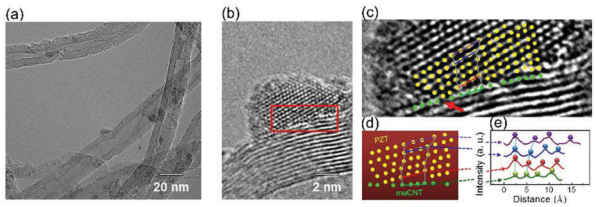

Fig. 31 (a) HRTEM images of epitaxial PZT-CNTs, (b) magnified image of the PZT nanoparticles, and (c) magnified image showing atomic arrangements and strain mismatch (d) atomic arrangement and (e) lattice spacing of PZT and mwCNTs. Adapted from Han *et al.*[169] with permission from Nature Publishing Group (Copyright 2016).

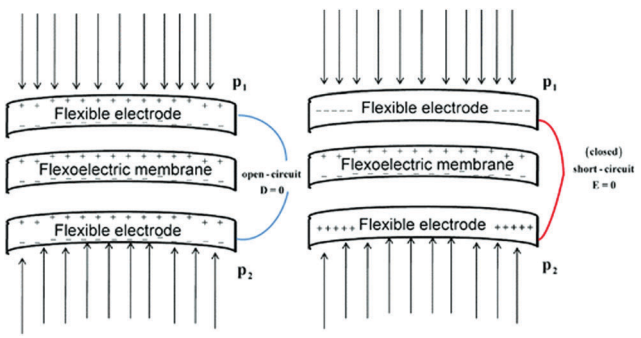

Fig. 32 Open ($D = 0$) and closed circuit ($E = 0$) states for a flexoelectric membrane under bending. P shows pressure. Reprinted figure with permission from ref. 153. Copyright (2013) by the American Physical Society.

harvesting that may be combined with, or even replace, piezoelectric systems. The size effect in this class of materials could provide self-powered integrated nano-systems that make use of mechanical forces in cells to manipulate their biological behaviour. In addition, flexoelectric based energy harvesting techniques offer efficient solutions in electrochemical recovery of ions such as calcium and lithium. For example, Trocoli *et al.* recently proposed a new method for lithium recovery from brines using an electro-chemical ion-pumping process.[171]

5.2 Flexo-electric effects in electro-chemical strain microscopy

Electro-chemical strain microscopy (ESM) is a new scanning probe microscopy (SPM) technique that enables local ionic flows and electrochemical reactions in solids to be probed and is based on flexoelectric and bias-strain coupling.[172,173] Fig. 33 shows an ESM measurement where the film being analysed is composed of mobile charged defects and electrons. The upper SPM tip produces an inhomogeneous electric field that leads to elastic strains that are proportional to the electric field gradient due to flexoelectric coupling. The redistribution of mobile charged particles influences the electric potential distribution in the film and induces local strains that are detected by the SPM tip; thereby providing electro-chemical information about the specimen.[174] The models developed that couple the electric–chemical–mechanical–thermal processes in this technique can also take into account bulk defect electro-chemical reactions – these new models may provide new insights where ion flow in a mechanical strain or electric field gradient can be used for nano-scale harvesting and storage.

5.3 Photo-flexo-electric effects

A photo-induced flexoelectric response was initially reported by Spassova for bilayer lipid membranes[175] and, recently, flexoelectricity has been reported to be responsible for light-induced current generation at structural boundaries between two phases of ferroelectric bismuth ferrite due to a coupling between strain gradient and photo-electric activity, see Fig. 34.[176] A localised light beam creates electron–hole pairs in the material and at grain boundary interfaces the electric fields from a strain gradient due to flexoelectric effect separates the two types of charge, and results in current flow normal to the interface.[177] Since the material is also piezoelectric there is potential to combine flexoelectric effects with the piezoelectric and photo-electro-chemical aspects described in Section 3.

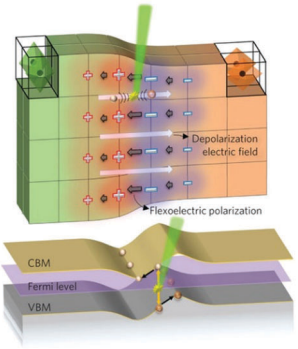

Fig. 34 Strain gradient at the interface of two different structural polymorphs induces a flexoelectric polarisation (dark arrows). Positive (red plus symbols) and negative (blue minus symbols) bound charges are produced which generate a depolarisation electric field (white arrows). This electric field is reflected in the electronic band bending (shown at image bottom). A photon creates an electron at or above the conduction band minimum (CBM) and a hole at or below the valence band maximum (VBM). These light-induced electron–hole pairs are separated before recombination owing because electrons and holes in an electric field move in opposite directions. Reprinted by permission from Macmillan Publishers Ltd: ref. 176, Copyright (2015).

6. Thermoelectric-chemical effects

Thermoelectrics are able to generate electrical energy from spatial thermal gradients, unlike pyroelectric materials that require temperatures that vary with time. Work on using thermoelectric power for water splitting has been reported as early as 1976,[178] where a hybrid thermo-chemical water-splitting cycle using solar energy was proposed which consisted of three subsystems. The first subsystem was a photochemical reaction ($2Fe^{2+} + I_3^- + \text{light} \rightarrow 2Fe^{3+} + 3I^-$) that was achieved in a flat cell through which the liquid reactant flowed. The cell was placed in direct sunlight above a Fresnel lens, as in Fig. 35 (upper right).

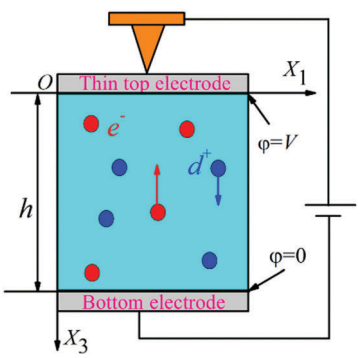

Fig. 33 Schematic of the electro-chemical processes at the tip–surface junction in electro-chemical strain microscopy. Reprinted from ref. 174 with permission of AIP Publishing.

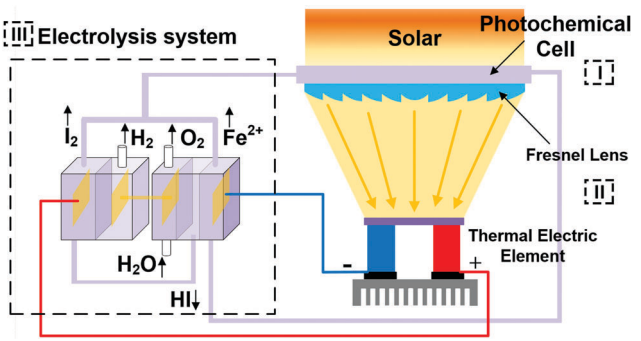

Fig. 35 Schematic of hybrid thermo-chemical water splitting, as described by ref. 178. Subsystem I is the photochemical cell. Subsystem II is the Fresnel lens and thermoelectric. Subsystem III is the electrolysis system.

The second subsystem was below the Fresnel lens where the remaining solar energy was concentrated onto a thermoelectric element. Cooling fins were used on the other side of the thermoelectric generator to maintain a temperature gradient. The final subsystem consisted of two electrolysers that combine the products of the photo-chemical reactions and electrolysis (Fig. 35, left). The overall efficiency was estimated as 15–25% with an initial production rate of one liter per hour of hydrogen was achieved;[178] further work[179] indicated that while the efficiency of the thermoelectric device is as low as 5%, the overall efficiency of hydrogen production can be raised to 20% by the additional electric power from the thermoelectric. Photo-electro-chemical (PEC) conversion of solar energy for water splitting has also used with thermoelectric devices. Self-biased water splitting was achieved by Jung *et al.* since the PEC system operated spontaneously on application of an overpotential generated by a thermoelectric. The system therefore allowed capture of both photons and waste heat and achieved a hydrogen power of 55 mW cm^{-2}.[181]

Chen *et al.*[180] reported a microbial electrolysis cell (MEC) to produce H_2 from acetate where an additional voltage was supplied by a thermoelectric to overcome the energy barrier, see Fig. 36. They showed that the thermoelectric microconverter could convert waste heat energy to electricity, even at relatively low temperature differences of 5 °C, and the hydrogen yield was increased from 1.05 to 2.7 mol mol^{-1} acetate and the coulombic efficiency increased from 27 to 83%. Rectification in not required for thermoelectrics since a unipolar output is achieved, provided the temperature gradient does not change sign. However, some conditioning of the voltage is necessary to ensure the voltage is at an appropriate output level since output voltages are typically low compared to the other harvesting approaches; see Table 1. Liu *et al.* have recently reported the coupling of both thermo-electricity and electro-catalysis for hydrogen production *via* a PbTe–PbS/TiO_2 heterojunction.[182] The triboelectric–thermoelectric–photovoltaic water splitting cell of Yang *et al.*[97] inspired an overview by Andrei *et al.*[183] on the potential for creating hybrid thermoelectric systems and the reader is referred to this excellent opinion article for additional details on thermoelectric devices for water splitting.

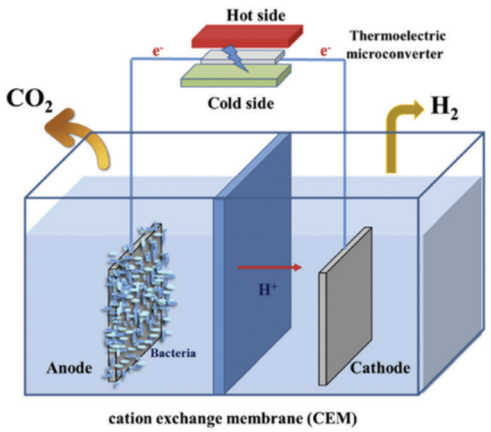

Fig. 36 Schematic of the coupled thermo-electric microbial electrolysis cell (MEC) system. Reprinted from ref. 180, Copyright(2016), with permission from Elsevier.

Electro-chemical effects in thermoelectric polymers are also attracting attention. Ion conducting materials have large Seebeck coefficients, and an advantage of polymers over inorganic materials is their high ionic conductivity at ambient temperature. As an example, poly(3,4-ethylene dioxythiophene):poly(styrene sulfonate), namely PEDOT:PSS, has demonstrated a large, but short-term increase, in Seebeck coefficient and Chang *et al.* has shown that the duration of the ionic Seebeck enhancement can be improved by controlling whether electro-chemistry occurs at the (PEDOT:PSS)/electrode interface.[184]

7. Photovoltaic-chemical coupling

Solar energy is an important renewable and efficient clean energy source, and significant effort has been made to couple this form of energy to electro-chemical systems. Since Fujishima *et al.* first reported photo-electro-chemical water splitting[185] and photo-reduction of CO_2[186] on TiO_2, in 1972 and 1979, respectively, numerous studies have focused on photo-catalytic materials and mechanisms, which have been summarised in a number of detailed reviews on the topic.[187–194] The impact of mechanical loads on the generation, separation, and recombination of photon-induced carriers has also been recently reviewed in the context of piezo-phototronic effects.[195]

As this review has a focus on the coupling of energy harvesting devices to electro-chemical systems, we will overview efforts on the use of photovoltaics as a power source for applications related to water splitting, CO_2 reduction and water treatment. Due to the relative maturity of solar cell technologies, power levels can be larger than the μW to mW range that is typical of 'energy harvesting' and can be in the W to MW range,[196] which is typical of 'energy generation'. Recent examples of emerging applications are now described.

As already highlighted for the piezo-, pyro- and tribo-electric systems, water splitting is a widely explored application to couple with solar harvesters.[185,197–207] In terms of the potential configurations for coupling a photovoltaic to an electro-chemical cell, Bonke *et al.*[197] illustrated three main approaches. This included a wireless, wired and modular photo-electro-chemical (PEC) system, as shown in Fig. 37 to achieve water splitting *via* eqn (1) and (2). The developed system employed the simple modular configuration in Fig. 37c, using nickel foam electrodes and a commercial GaInP/GaAs/Ge multi-junction photovoltaic module with a solar-to-electrical power conversion efficiency of 37% under concentrated solar conditions. By optimizing the electrode material, electrode size, electrolyser conditions and using concentrated solar power the solar-energy to fuel-energy conversion efficiency was 22.4%, which was higher than previously reported results that were typically 10–18%. Solar cells have also been coupled to a proton-exchange membrane (PEM) electrolyser to generate hydrogen, with a maximum efficiency of 16.8%.[204,205,208]

Another promising approach is the electro-chemical reduction of CO_2 into fuels.[186,209–213] Schreier *et al.*[209] used

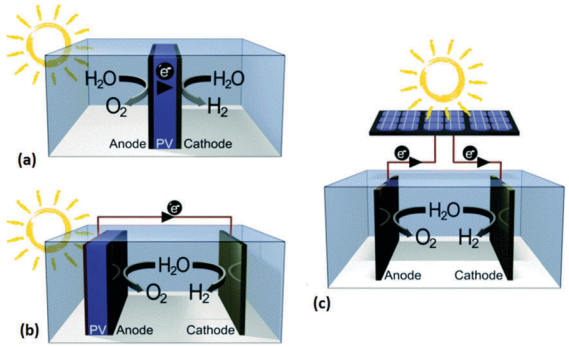

Fig. 37 Schematic of light-driven water electrolysis approaches. (a) Fully integrated and wireless photo-electro-chemical (PEC) system; (b) partially integrated and wired PEC; (c) non-integrated and modular PEC. Reproduced from ref. 197 with permission from The Royal Society of Chemistry.

atomic layer deposition of SnO_2 on CuO nanowires to produce a catalyst for CO_2 reduction to CO, which was then combined with a triple junction GaInP/GaInAs/Ge photovoltaic cell (PV cell). This is shown in Fig. 38, which also shows a bipolar membrane as the separator to allow for operation using a different catholyte and anolyte. Surface modification of the CuO nanowire electrodes with SnO_2 provided improved selectivity of the catalyst, and the solar cell was used to drive the electro-chemical reaction between the anode and cathode. Photolysis of CO_2 with a peak solar-to-CO free-energy conversion efficiency of 13.4% was achieved in a system that used far more abundant and lower-cost materials, as compared to other approaches that employed noble metals.

An additional application is the use of photovoltaic cells for water treatment.[214–219] Wang *et al.*[219] have recently reported a hybrid photovoltaic-solar water disinfection system with a dual-axis tracking system to provide drinkable water and renewable electricity. Fig. 39 shows a schematic of the hybrid system, where the use of a V-trough concentrator was found to significantly improve the sterilisation efficiency compared to a non-concentrating system; the addition of H_2O_2 to the water also

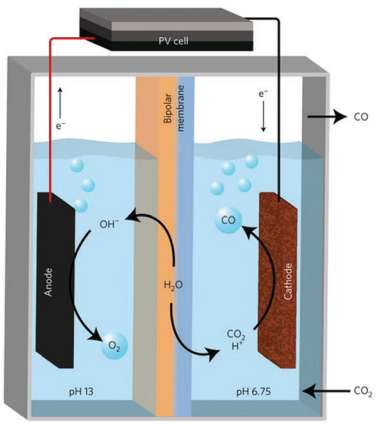

Fig. 38 Schematic of solar-driven CO_2 reduction device. Anode: reaction: $2OH^- \rightarrow H_2O + \frac{1}{2}O_2 + 2e^-$; cathode reaction: $CO_2 + 2H^+ + 2e^- \rightarrow CO + H_2O$. Reprinted by permission from Macmillan Publishers Ltd: ref. 209 (Copyright 2017).

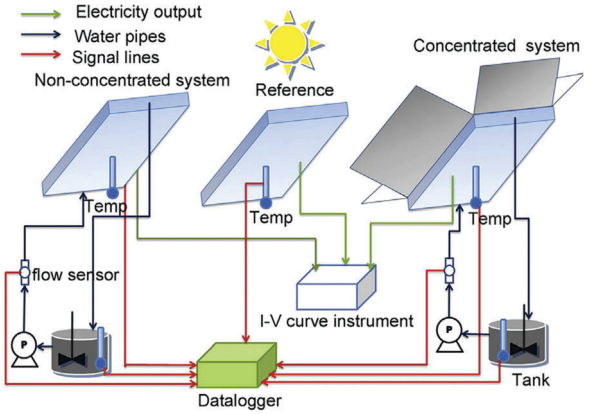

Fig. 39 Schematic of hybrid photovoltaic solar water disinfection system. Reprinted from ref. 219. Copyright (2016), with permission from Elsevier.

aided disinfection. Two types of bacteria, *Salmonella* and *Escherichia coli*, were evaluated and it was demonstrated that they were completely inactivated in 2.5 h and 1.25 h respectively. As with piezo- and tribo-electric systems, photovoltaics have also be used for corrosion protection, such as electro-chemical chloride extraction in concrete;[220] electro-chemical refrigeration[221] has also been explored.

8. Conclusions and perspectives

This review has covered in detail the progress to date on energy harvesting based on piezoelectric, pyroelectric triboelectric, flexoelectric, thermoelectric and photovoltaic effects that are coupled to electro-chemical systems. Table 1 provides a summary of the harvesting approaches and potential applications which cover a wide range of electro-chemical processes including water splitting, water treatment such as disinfection and degradation of pollutants, corrosion protection, materials synthesis including electro-deposition and oxidation, sensing and electro-chromic systems. The energy sources are varied and include thermal, solar/light, wave/water flow, wind, vibrations and mechanical loads; hybrid systems are also being developed to overcome the intermittent nature of some ambient sources of energy. Since a number of harvesting mechanisms generate AC electrical outputs in response to compressive/tensile loads or heating/cooling cycles some form of rectification is often required to maintain a unipolar operation when the harvester is coupled to cathodes and anodes. Voltage transformation, typically to reduce the high voltages generated by tribo- & piezo-electric (see Table 1), is also required; although if the generated potential is too low to drive a specific electro-chemical reaction there is scope to increase the operating voltage. While the voltages are high (typically 0.02 V to 1.3 kV) to drive the electro-chemical reaction, currents are often low (14.5 μA to 13 mA) which limits the charge and extent of the electro-chemical reaction (eqn (3)); although there is growing interest in potential for scale up.[222] To date, rectification methods applied to electro-chemical systems have been relatively simple, such as simple diode and full wave rectification, while in conventional harvesting applications a range power management circuits

have been developed to minimise losses and optimise impedance matching of the harvester to the electrical load; this provides scope for further improvement in the electro-chemical applications.[223] Greater information regarding overall efficiencies of systems would also be of interest. For solar harvesting, the system efficiencies are more widely reported, and the other harvesting approaches would benefit from similar information. Solar is also typically associated with larger harvesting systems. Tribo-electric devices have been typically used as an external charge source to drive an electro-chemical reaction since a complete TENG device is typically required to achieve charge generation. However, for pyro- and piezo-electric systems the inherent spontaneous polarisation of the material enables them to be either used as an external thermal or vibration harvesting device or as fine particulates or porous material dispersed in an electrolyte. This is of interest since it enables the high surface areas (and therefore surface charge) associated with nano-sized particulates and architectures. This provides an opportunity to overcome the low electric current/charge limitations in Table 1. The potential to exploit the high surface area of 2D materials, and their ability to also exhibit flexoelectric effects, is also of interest. A closer integration of TENGs with electrolytes may provide new directions for research and triboelectric effects associated with electrical double layers has recently been reported in novel sensing tribo-devices.[224]

There is also potential to combine the active harvesting material with storage, as an example the understanding of the pyro- and piezo-electric properties of metal–organic frameworks (MOFs) is growing,[225] and these materials also have potential for gas storage applications so that combined harvesting for hydrogen production and storage may be feasible. The potential of pyro-electric effects to achieve water splitting by thermal cycling above and below the Curie temperature is a new and exciting prospect for hydrogen generation, but experimental data is needed to validation model predictions and mechanisms.

Flexo-electric systems are clearly at an early stage, but their scope for nano-scale systems and ability to exploit membrane effects provides intriguing potential for membrane based nano-generators combined with ion pumping for charge storage applications. There is also scope for using strain gradients and flexoelectric effects at interfaces to influence and enhance photo-flexo-electro-chemical effects and subjecting the materials to mechanical loads or thermal expansion. Ferro-electrets or electro-active polymers could also be explored, and there has been limited work on electro-magnetic harvesting. Hybrid systems that use the DC output of thermoelectric modules are attractive due to their ability to supply overpotentials to electro-chemical reactions and new thermoelectric polymers and nanocomposites also provide new directions.[226,227] There are also additional electro-chemical harvesting mechanisms to couple with the harvesting approaches described here. For example, there are sensitised thermal cells, thermo-galvanic and thermo-electro-chemical cells (thermocells),[228–235] where the dependence of electrode potential on temperature is used to construct harvesting thermal cycles and this has recently been reviewed.[236] Piezo-galvanic effects have even been observed where applying an asymmetric force to an electrolyte cell produces an electrical response[237] and thermo-magnetic effects for water splitting.[238]

Finally a number of new electro-chemical processes could be explored in attempt to exploit the high voltages of the energy harvesting mechanism described in this review; such as material synthesis based on electro-chemical exfoliation.[239] The potential of local energy harvesting to supply bioreactors to produce protein as a food source has recently been described.[240] Finally, while there is a growing number of academic publications, and patents, there is also a need to transfer such ideas and potential applications into commercial activities to fully exploit the potential of the applications described here.

Conflicts of interest

There are no conflicts to declare.

Acknowledgements

Dr Y. Zhang would like to acknowledge the European Commission's Marie Skłodowska-Curie Actions (MSCA), through the Marie Skłodowska-Curie Individual Fellowships (IF-EF) (H2020-MSCA-IF-2015-EF-703950-HEAPPs) under Horizon 2020. Prof. C. R. Bowen, Dr M. Xie and Dr V. Adamaki would like to acknowledge the funding from the European Research Council under the European Union's Seventh Framework Programme (FP/2007–2013)/ERC Grant Agreement No. 320963 on Novel Energy Materials, Engineering Science and Integrated Systems (NEMESIS).

Notes and references

1 A. Vlad, N. Singh, C. Galande and P. M. Ajayan, *Adv. Energy Mater.*, 2015, **5**, 1402115.
2 H. Wei, D. Cui, J. Ma, L. Chu, X. Zhao, H. Song, H. Liu, T. Liu, N. Wang and Z. Guo, *J. Mater. Chem. A*, 2017, **5**, 1873–1894.
3 Y. Zhong, X. H. Xia, W. J. Mai, J. P. Tu and H. J. Fan, *Adv. Mater. Technol.*, 2017, 1700182.
4 J.-H. Lee, J. Kim, T. Y. Kim, M. S. Al Hossain, S.-W. Kim and J. H. Kim, *J. Mater. Chem. A*, 2016, **4**, 7983–7999.
5 C. R. Bowen, J. Taylor, E. LeBoulbar, D. Zabek, A. Chauhan and R. Vaish, *Energy Environ. Sci.*, 2014, **7**, 3836–3856.
6 C. R. Bowen, H. A. Kim, P. M. Weaver and S. Dunn, *Energy Environ. Sci.*, 2014, **7**, 25–44.
7 Z. L. Wang, *Mater. Today*, 2017, **20**, 74–82.
8 Z. L. Wang, *Faraday Discuss.*, 2014, **176**, 447–458.
9 G. Tan, L.-D. Zhao and M. G. Kanatzidis, *Chem. Rev.*, 2016, **116**, 12123–12149.
10 P. Zubko, G. Catalan and A. K. Tagantsev, *Annu. Rev. Mater. Res.*, 2013, **43**, 387–421.
11 F. Invernizzi, S. Dulio, M. Patrini, G. Guizzetti and P. Mustarelli, *Chem. Soc. Rev.*, 2016, **45**, 5455–5473.
12 R. E. Blankenship, D. M. Tiede, J. Barber, G. W. Brudvig, G. Fleming, M. Ghirardi, M. R. Gunner, W. Junge,

D. M. Kramer, A. Melis, T. A. Moore, C. C. Moser, D. G. Nocera, A. J. Nozik, D. R. Ort, W. W. Parson, R. C. Prince and R. T. Sayre, *Science*, 2011, **332**, 805–809.
13 A. Shiroudi, M. S. Deleuze and S. A. Mousavifar, *Int. J. Ambient Energy*, 2017, **38**, 240–249.
14 A. Mostafaeipour, M. Khayyami, A. Sedaghat, K. Mohammadi, S. Shamshirband, M.-A. Sehati and E. Gorakifard, *Int. J. Hydrogen Energy*, 2016, **41**, 6200–6210.
15 M. Qolipour, A. Mostafaeipour and O. M. Tousi, *Renewable Sustainable Energy Rev.*, 2017, **78**, 113–123.
16 R. M. Navarro, M. A. Peña and J. L. G. Fierro, *Chem. Rev.*, 2007, **107**, 3952–3991.
17 A. Kudo and Y. Miseki, *Chem. Soc. Rev.*, 2009, **38**, 253–278.
18 Y. Zheng, Y. Jiao, M. Jaroniec and S. Z. Qiao, *Angew. Chem., Int. Ed.*, 2015, **54**, 52–65.
19 V. Artero, M. Chavarot-Kerlidou and M. Fontecave, *Angew. Chem., Int. Ed.*, 2011, **50**, 7238–7266.
20 M. Xie, S. Dunn, E. L. Boulbar and C. R. Bowen, *Int. J. Hydrogen Energy*, 2017, **42**, 23437–23445.
21 M. Baldauf, T. Hammer, S. Kosse and G. Zimmermann, *Germany Pat.*, WO 2012110352 A1, 2012.
22 C. Cherkouk, M. Zschornak, J. Hanzig, M. Nentwich, F. Meutzner, M. Urena, T. Leisegang and D. C. Meyer, *COMSOL multiphysics® simulation of energy conversion and storage concepts based on oxide crystals*, 2014.
23 R. Belitz, P. Meisner, M. Coeler, U. Wunderwald, J. Friedrich, J. Zosel, M. Schelter, S. Jachalke and E. Mehner, *Energy Harv. Syst.*, 2017, DOI: 10.1515/ehs-2016-0009.
24 S. Habicht, R. J. Nemanich and A. Gruverman, *Nanotechnology*, 2008, **19**, 495303.
25 A. Kakekhani, S. Ismail-Beigi and E. I. Altman, *Surf. Sci.*, 2016, **650**, 302–316.
26 A. Kakekhani and S. Ismail-Beigi, *ACS Catal.*, 2015, **5**, 4537–4545.
27 A. Kakekhani and S. Ismail-Beigi, *Phys. Chem. Chem. Phys.*, 2016, **18**, 19676–19695.
28 A. Kakekhani and S. Ismail-Beigi, *J. Mater. Chem. A*, 2016, **4**, 5235–5246.
29 X.-W. Liu, W.-W. Li and H.-Q. Yu, *Chem. Soc. Rev.*, 2014, **43**, 7718–7745.
30 T. F. Wiesner, *Pyroelectrically-mediated reduction–oxidation reactions*, Texas Tech University, 2010.
31 E. Gutmann, A. Benke, K. Gerth, H. Böttcher, E. Mehner, C. Klein, U. Krause-Buchholz, U. Bergmann, W. Pompe and D. C. Meyer, *J. Phys. Chem. C*, 2012, **116**, 5383–5393.
32 A. Benke, E. Mehner, M. Rosenkranz, E. Dmitrieva, T. Leisegang, H. Stöcker, W. Pompe and D. C. Meyer, *J. Phys. Chem. C*, 2015, **119**, 18278–18286.
33 J. Wu, W. Mao, Z. Wu, X. Xu, H. You, A. X. Xue and Y. Jia, *Nanoscale*, 2016, **8**, 7343–7350.
34 Y. Xia, Y. Jia, W. Qian, X. Xu, Z. Wu, Z. Han, Y. Hong, H. You, M. Ismail, G. Bai and L. Wang, *Metals*, 2017, **7**, 122.
35 W. Qian, Z. Wu, Y. Jia, Y. Hong, X. Xu, H. You, Y. Zheng and Y. Xia, *Electrochem. Commun.*, 2017, **81**, 124–127.
36 C. Forman, M. Gootz, D. Scheithauer, M. Herrmann, E. Mehner, B. Meyer, D. C. Meyer, I. Muritala, R. Pardemann and O. Schulze, *European Pat.*, EP 3027551 A2, 2016.
37 Y. Yang, H. Zhang, S. Lee, D. Kim, W. Hwang and Z. L. Wang, *Nano Lett.*, 2013, **13**, 803–808.
38 H. Zhang, S. Zhang, G. Yao, Z. Huang, Y. Xie, Y. Su, W. Yang, C. Zheng and Y. Lin, *ACS Appl. Mater. Interfaces*, 2015, **7**, 28142–28147.
39 T. Zhao, W. Jiang, D. Niu, H. Liu, B. Chen, Y. Shi, L. Yin and B. Lu, *Appl. Energy*, 2017, **195**, 754–760.
40 R. W. Salt, *Science*, 1961, **133**, 458–459.
41 D. Ehre, E. Lavert, M. Lahav and I. Lubomirsky, *Science*, 2010, **327**, 672.
42 D. Spitzner, U. Bergmann, S. Apelt, R. Boucher and H.-P. Wiesmann, *Coatings*, 2015, **5**, 724.
43 S. Piperno, E. Mirzadeh, E. Mishuk, D. Ehre, S. Cohen, M. Eisenstein, M. Lahav and I. Lubomirsky, *Angew. Chem., Int. Ed.*, 2013, **52**, 6513–6516.
44 A. Pichon, *Nat. Chem.*, 2013, **5**, 551.
45 D. Ehre, B. Alik, E. Mishuk, M. Lahav and I. Lubomirsky, *Proceedings of the 2014 ESA Annual Meeting on Electrostatics*, 2014.
46 S. Coppola, *Manipulation of Multiphase Materials for Touch-less Nanobiotechnology: A Pyrofluidic Platform*, Springer International Publishing, Cham, 2016, pp. 5–22, DOI: 10.1007/978-3-319-31059-6_2.
47 X. Xi, D. Zhao, F. Tong and T. Cao, *Soft Matter*, 2012, **8**, 298–302.
48 S. Grilli, L. Miccio, V. Vespini, A. Finizio, S. De Nicola and P. Ferraro, *Opt. Express*, 2008, **16**, 8084–8093.
49 K.-S. Hong, H. Xu, H. Konishi and X. Li, *J. Phys. Chem. Lett.*, 2010, **1**, 997–1002.
50 M. B. Starr and X. Wang, *Nano Energy*, 2015, **14**, 296–311.
51 M. B. Starr and X. Wang, *Sci. Rep.*, 2013, **3**, 2160.
52 M. B. Starr, J. Shi and X. Wang, *Angew. Chem., Int. Ed.*, 2012, **51**, 5962–5966.
53 M. E. Lines and A. M. Glass, *Principles and Applications of Ferroelectrics and Related Materials*, Oxford Scholarship Online, 2001.
54 J. Zhang, Z. Wu, Y. Jia, J. Kan and G. Cheng, *Sensors*, 2013, **13**, 367.
55 C. F. Tan, W. L. Ong and G. W. Ho, *ACS Nano*, 2015, **9**, 7661–7670.
56 W. Yang, Y. Yu, M. B. Starr, X. Yin, Z. Li, A. Kvit, S. Wang, P. Zhao and X. Wang, *Nano Lett.*, 2015, **15**, 7574–7580.
57 K.-S. Hong, H. Xu, H. Konishi and X. Li, *J. Phys. Chem. C*, 2012, **116**, 13045–13051.
58 H. Lin, Z. Wu, Y. Jia, W. Li, R.-K. Zheng and H. Luo, *Appl. Phys. Lett.*, 2014, **104**, 162907.
59 W. Lv, L. Kong, S. Lan, J. Feng, Y. Xiong and S. Tian, *J. Chem. Technol. Biotechnol.*, 2017, **92**, 152–156.
60 Z. L. Wang, *Nano Today*, 2010, **5**, 540–552.
61 X. Xue, W. Zang, P. Deng, Q. Wang, L. Xing, Y. Zhang and Z. L. Wang, *Nano Energy*, 2015, **13**, 414–422.
62 M.-K. Lo, S.-Y. Lee and K.-S. Chang, *J. Phys. Chem. C*, 2015, **119**, 5218–5224.

63 Y.-T. Wang and K.-S. Chang, *J. Am. Ceram. Soc.*, 2016, **99**, 2593–2600.
64 D. Hong, W. Zang, X. Guo, Y. Fu, H. He, J. Sun, L. Xing, B. Liu and X. Xue, *ACS Appl. Mater. Interfaces*, 2016, **8**, 21302–21314.
65 C. Sun, Y. Fu, Q. Wang, L. Xing, B. Liu and X. Xue, *RSC Adv.*, 2016, **6**, 87446–87453.
66 H. Li, Y. Sang, S. Chang, X. Huang, Y. Zhang, R. Yang, H. Jiang, H. Liu and Z. L. Wang, *Nano Lett.*, 2015, **15**, 2372–2379.
67 M. A. Khan, M. A. Nadeem and H. Idriss, *Surf. Sci. Rep.*, 2016, **71**, 1–31.
68 Y. Cui, J. Briscoe and S. Dunn, *Chem. Mater.*, 2013, **25**, 4215–4223.
69 Y. Cui, S. M. Goldup and S. Dunn, *RSC Adv.*, 2015, **5**, 30372–30379.
70 P. M. Jones and S. Dunn, *J. Phys. D: Appl. Phys.*, 2009, **42**, 065408.
71 P. M. Jones and S. Dunn, *Nanotechnology*, 2007, **18**, 185702.
72 M. Stock and S. Dunn, *IEEE Trans. Ultrason. Ferroelectr. Freq. Control*, 2011, **58**, 1988–1993.
73 M. Stock and S. Dunn, *J. Phys. Chem. C*, 2012, **116**, 20854–20859.
74 D. Tiwari and S. Dunn, *Mater. Lett.*, 2012, **79**, 18–20.
75 X. Xue, S. Wang, W. Guo, Y. Zhang and Z. L. Wang, *Nano Lett.*, 2012, **12**, 5048–5054.
76 X. Xue, P. Deng, S. Yuan, Y. Nie, B. He, L. Xing and Y. Zhang, *Energy Environ. Sci.*, 2013, **6**, 2615–2620.
77 Y.-S. Kim, Y. Xie, X. Wen, S. Wang, S. J. Kim, H.-K. Song and Z. L. Wang, *Nano Energy*, 2015, **14**, 77–86.
78 L. Xing, Y. Nie, X. Xue and Y. Zhang, *Nano Energy*, 2014, **10**, 44–52.
79 Z. Yan, Z. Yujing, X. Xinyu, C. Chunxiao, H. Bin, N. Yuxin, D. Ping and W. Zhong Lin, *Nanotechnology*, 2014, **25**, 105401.
80 A. Ramadoss, B. Saravanakumar, S. W. Lee, Y.-S. Kim, S. J. Kim and Z. L. Wang, *ACS Nano*, 2015, **9**, 4337–4345.
81 R. Song, H. Jin, X. Li, L. Fei, Y. Zhao, H. Huang, H. L.-W. Chan, Y. Wang and Y. Chai, *J. Mater. Chem. A*, 2015, **3**, 14963–14970.
82 F. Wang, C. Jiang, C. Tang, S. Bi, Q. Wang, D. Du and J. Song, *Nano Energy*, 2016, **21**, 209–216.
83 K. Parida, V. Bhavanasi, V. Kumar, J. Wang and P. S. Lee, *J. Power Sources*, 2017, **342**, 70–78.
84 B.-S. Lee, J. Yoon, C. Jung, D. Y. Kim, S.-Y. Jeon, K.-H. Kim, J.-H. Park, H. Park, K. H. Lee, Y.-S. Kang, J.-H. Park, H. Jung, W.-R. Yu and S.-G. Doo, *ACS Nano*, 2016, **10**, 2617–2627.
85 S. Kim, S. J. Choi, K. Zhao, H. Yang, G. Gobbi, S. Zhang and J. Li, *Nat. Commun.*, 2016, **7**, 10146.
86 K. Noris-Suárez, J. Lira-Olivares, A. M. Ferreira, A. Graterol, J. L. Feijoo and W. S. Lee, *Mater. Sci. Forum*, 2007, **544–545**, 981–984.
87 S. B. Lang, S. A. M. Tofail, A. L. Kholkin, M. Wojtaś, M. Gregor, A. A. Gandhi, Y. Wang, S. Bauer, M. Krause and A. Plecenik, *Sci. Rep.*, 2013, **3**, 2215.
88 F. R. Baxter, C. R. Bowen, I. G. Turner and A. C. E. Dent, *Ann. Biomed. Eng.*, 2010, **38**, 2079–2092.
89 P. Soroushian, R.-U.-D. Nassar and A. M. Balachandra, *J. Intell. Mater. Syst.*, 2013, **24**, 441–453.
90 N. Touach, V. M. Ortiz-Martínez, M. J. Salar-García, A. Benzaouak, F. Hernández-Fernández, A. P. de Ríos, M. El Mahi and E. M. Lotfi, *Particuology*, 2017, **34**, 147–155.
91 F.-R. Fan, Z.-Q. Tian and Z. Lin Wang, *Nano Energy*, 2012, **1**, 328–334.
92 G. Zhu, Y. S. Zhou, P. Bai, X. S. Meng, Q. Jing, J. Chen and Z. L. Wang, *Adv. Mater.*, 2014, **26**, 3788–3796.
93 W. Tang, T. Jiang, F. R. Fan, A. F. Yu, C. Zhang, X. Cao and Z. L. Wang, *Adv. Funct. Mater.*, 2015, **25**, 3718–3725.
94 Z. L. Wang, T. Jiang and L. Xu, *Nano Energy*, 2017, **39**, 9–23.
95 X. Cao, Y. Jie, N. Wang and Z. L. Wang, *Adv. Energy Mater.*, 2016, **6**, 1600665.
96 W. Tang, Y. Han, C. B. Han, C. Z. Gao, X. Cao and Z. L. Wang, *Adv. Mater.*, 2015, **27**, 272–276.
97 Y. Yang, H. Zhang, Z.-H. Lin, Y. Liu, J. Chen, Z. Lin, Y. S. Zhou, C. P. Wong and Z. L. Wang, *Energy Environ. Sci.*, 2013, **6**, 2429–2434.
98 S. A. Nahian, R. K. Cheedarala and K. K. Ahn, *Nano Energy*, 2017, **38**, 447–456.
99 X. Yu, X. Han, Z. Zhao, J. Zhang, W. Guo, C. Pan, A. Li, H. Liu and Z. Lin Wang, *Nano Energy*, 2015, **11**, 19–27.
100 W. Zhou, Z. Yin, Y. Du, X. Huang, Z. Zeng, Z. Fan, H. Liu, J. Wang and H. Zhang, *Small*, 2013, **9**, 140–147.
101 T. Li, Y. Xu, F. Xing, X. Cao, J. Bian, N. Wang and Z. L. Wang, *Adv. Energy Mater.*, 2017, **7**, 1700124.
102 Y.-C. Pu, G. Wang, K.-D. Chang, Y. Ling, Y.-K. Lin, B. C. Fitzmorris, C.-M. Liu, X. Lu, Y. Tong, J. Z. Zhang, Y.-J. Hsu and Y. Li, *Nano Lett.*, 2013, **13**, 3817–3823.
103 P. Song, S. Kuang, N. Panwar, G. Yang, D. J. H. Tng, S. C. Tjin, W. J. Ng, M. B. A. Majid, G. Zhu, K.-T. Yong and Z. L. Wang, *Adv. Mater.*, 2017, **29**, 1605668.
104 S. Yuanjie, Y. Ya, Z. Hulin, X. Yannan, W. Zhiming, J. Yadong, F. Naoki, B. Yoshio and W. Zhong Lin, *Nanotechnology*, 2013, **24**, 295401.
105 Y. Yang, H. Zhang, Y. Liu, Z.-H. Lin, S. Lee, Z. Lin, C. P. Wong and Z. L. Wang, *ACS Nano*, 2013, **7**, 2808–2813.
106 Q. Jiang, Y. Han, W. Tang, H. Zhu, C. Gao, S. Chen, M. Willander, X. Cao and Z. Lin Wang, *Nano Energy*, 2015, **15**, 266–274.
107 Z. Li, J. Chen, J. Yang, Y. Su, X. Fan, Y. Wu, C. Yu and Z. L. Wang, *Energy Environ. Sci.*, 2015, **8**, 887–896.
108 Q. Jiang, Y. Jie, Y. Han, C. Gao, H. Zhu, M. Willander, X. Zhang and X. Cao, *Nano Energy*, 2015, **18**, 81–88.
109 S. Chen, C. Gao, W. Tang, H. Zhu, Y. Han, Q. Jiang, T. Li, X. Cao and Z. Wang, *Nano Energy*, 2015, **14**, 217–225.
110 X. Zheng, J. Su, X. Wei, T. Jiang, S. Gao and Z. L. Wang, *Adv. Mater.*, 2016, **28**, 5188–5194.
111 S. Gao, J. Su, M. Wang, X. Wei, X. Zheng and T. Jiang, *Nano Energy*, 2016, **30**, 52–58.
112 S. Gao, J. Su, X. Wei, M. Wang, M. Tian, T. Jiang and Z. L. Wang, *ACS Nano*, 2017, **11**, 770–778.

113 S. Gao, Y. Chen, J. Su, M. Wang, X. Wei, T. Jiang and Z. L. Wang, *ACS Nano*, 2017, **11**, 3965–3972.
114 G. Chen, *Sep. Purif. Technol.*, 2004, **38**, 11–41.
115 S. Chen, N. Wang, L. Ma, T. Li, M. Willander, Y. Jie, X. Cao and Z. L. Wang, *Adv. Energy Mater.*, 2016, **6**, 1501778.
116 M.-H. Yeh, H. Guo, L. Lin, Z. Wen, Z. Li, C. Hu and Z. L. Wang, *Adv. Funct. Mater.*, 2016, **26**, 1054–1062.
117 S.-B. Jeon, S. Kim, S.-J. Park, M.-L. Seol, D. Kim, Y. K. Chang and Y.-K. Choi, *Nano Energy*, 2016, **28**, 288–295.
118 Z. Li, J. Chen, J. Zhou, L. Zheng, K. C. Pradel, X. Fan, H. Guo, Z. Wen, M.-H. Yeh, C. Yu and Z. L. Wang, *Nano Energy*, 2016, **22**, 548–557.
119 X. J. Zhao, G. Zhu, Y. J. Fan, H. Y. Li and Z. L. Wang, *ACS Nano*, 2015, **9**, 7671–7677.
120 W. Guo, X. Li, M. Chen, L. Xu, L. Dong, X. Cao, W. Tang, J. Zhu, C. Lin, C. Pan and Z. L. Wang, *Adv. Funct. Mater.*, 2014, **24**, 6691–6699.
121 X. Li, J. Tao, W. Guo, X. Zhang, J. Luo, M. Chen, J. Zhu and C. Pan, *J. Mater. Chem. A*, 2015, **3**, 22663–22668.
122 Z. Wang, L. Cheng, Y. Zheng, Y. Qin and Z. L. Wang, *Nano Energy*, 2014, **10**, 37–43.
123 H. R. Zhu, W. Tang, C. Z. Gao, Y. Han, T. Li, X. Cao and Z. L. Wang, *Nano Energy*, 2015, **14**, 193–200.
124 Y. Feng, Y. Zheng, Z. U. Rahman, D. Wang, F. Zhou and W. Liu, *J. Mater. Chem. A*, 2016, **4**, 18022–18030.
125 S. Cui, Y. Zheng, J. Liang and D. Wang, *Chem. Sci.*, 2016, **7**, 6477–6483.
126 G. Zhu, C. Pan, W. Guo, C.-Y. Chen, Y. Zhou, R. Yu and Z. L. Wang, *Nano Lett.*, 2012, **12**, 4960–4965.
127 J. Wang, Z. Wen, Y. Zi, P. Zhou, J. Lin, H. Guo, Y. Xu and Z. L. Wang, *Adv. Funct. Mater.*, 2016, **26**, 1070–1076.
128 J. Wang, Z. Wen, Y. Zi, L. Lin, C. Wu, H. Guo, Y. Xi, Y. Xu and Z. L. Wang, *Adv. Funct. Mater.*, 2016, **26**, 3542–3548.
129 H. Zhu, Y. Xu, Y. Han, S. Chen, T. Zhou, M. Willander, X. Cao and Z. Wang, *Nano Res.*, 2015, **8**, 3604–3611.
130 Y. Jie, N. Wang, X. Cao, Y. Xu, T. Li, X. Zhang and Z. L. Wang, *ACS Nano*, 2015, **9**, 8376–8383.
131 Z. Li, J. Chen, H. Guo, X. Fan, Z. Wen, M. H. Yeh, C. Yu, X. Cao and Z. L. Wang, *Adv. Mater.*, 2016, **28**, 2983–2991.
132 Z. H. Lin, G. Zhu, Y. S. Zhou, Y. Yang, P. Bai, J. Chen and Z. L. Wang, *Angew. Chem., Int. Ed.*, 2013, **52**, 5065–5069.
133 Z. Wen, J. Chen, M.-H. Yeh, H. Guo, Z. Li, X. Fan, T. Zhang, L. Zhu and Z. L. Wang, *Nano Energy*, 2015, **16**, 38–46.
134 H. Zhang, Y. Yang, T.-C. Hou, Y. Su, C. Hu and Z. L. Wang, *Nano Energy*, 2013, **2**, 1019–1024.
135 H. Zhang, Y. Yang, Y. Su, J. Chen, C. Hu, Z. Wu, Y. Liu, C. Ping Wong, Y. Bando and Z. L. Wang, *Nano Energy*, 2013, **2**, 693–701.
136 X. Yang, G. Zhu, S. Wang, R. Zhang, L. Lin, W. Wu and Z. L. Wang, *Energy Environ. Sci.*, 2012, **5**, 9462–9466.
137 Y. Song, X. Cheng, H. Chen, J. Huang, X. Chen, M. Han, Z. Su, B. Meng, Z. Song and H. Zhang, *J. Mater. Chem. A*, 2016, **4**, 14298–14306.
138 J.-G. Sun, T. N. Yang, I. S. Kuo, J.-M. Wu, C.-Y. Wang and L.-J. Chen, *Nano Energy*, 2017, **32**, 180–186.
139 M.-H. Yeh, L. Lin, P.-K. Yang and Z. L. Wang, *ACS Nano*, 2015, **9**, 4757–4765.
140 F. Zhang, B. Li, J. Zheng and C. Xu, *Nanoscale Res. Lett.*, 2015, **10**, 298.
141 M. Zhang, Y. Jie, X. Cao, J. Bian, T. Li, N. Wang and Z. L. Wang, *Nano Energy*, 2016, **30**, 155–161.
142 Y.-K. Fuh, S.-C. Li and C.-Y. Chen, *APL Mater.*, 2017, **5**, 074202.
143 Y. Su, G. Xie, S. Wang, H. Tai, Q. Zhang, H. Du, H. Zhang, X. Du and Y. Jiang, *Sens. Actuators, B*, 2017, **251**, 144–152.
144 H. Zhu, N. Wang, Y. Xu, S. Chen, M. Willander, X. Cao and Z. L. Wang, *Adv. Funct. Mater.*, 2016, **26**, 3029–3035.
145 Y. Zheng, L. Cheng, M. Yuan, Z. Wang, L. Zhang, Y. Qin and T. Jing, *Nanoscale*, 2014, **6**, 7842–7846.
146 L. Su, H. Y. Li, Y. Wang, S. Y. Kuang, Z. L. Wang and G. Zhu, *Nano Energy*, 2017, **31**, 264–269.
147 J.-G. Sun, T. N. Yang, I.-S. Kuo, J.-M. Wu, C.-Y. Wang and L.-J. Chen, *Nano Energy*, 2017, **32**, 180–186.
148 A. G. Petrov, *Biochim. Biophys. Acta*, 2002, **1561**, 1–25.
149 A. Todorov, A. Petrov and J. Fendler, *J. Phys. Chem.*, 1994, **98**, 3076–3079.
150 Z. Ping-Cheng, A. M. Keleshian and F. Sachs, *Nature*, 2001, **413**, 428.
151 J. Mosbacher, M. Langer, J. Hörber and F. Sachs, *J. Gen. Physiol.*, 1998, **111**, 65–74.
152 A. G. Petrov, in *Physical and Chemical Bases of Biological Information Transfer*, ed. J. G. Vassileva-Popova, Plenum Press, New York, 1975, vol. 111.
153 A. D. Rey, P. Servio and E. Herrera-Valencia, *Phys. Rev. E: Stat., Nonlinear, Soft Matter Phys.*, 2013, **87**, 022505.
154 F. Ahmadpoor, Q. Deng, L. Liu and P. Sharma, *Phys. Rev. E: Stat., Nonlinear, Soft Matter Phys.*, 2013, **88**, 050701.
155 A. G. Petrov, B. A. Miller, K. Hristova and P. N. Usherwood, *Eur. Biophys. J.*, 1993, **22**, 289–300.
156 A. G. Petrov, *Anal. Chim. Acta*, 2006, **568**, 70–83.
157 A. G. Petrov and P. N. Usherwood, *Eur. Biophys. J.*, 1994, **23**, 1–19.
158 F. Ahmadpoor and P. Sharma, *Nanoscale*, 2015, **7**, 16555–16570.
159 A. Petrov and L. Mircevova, *Gen. Physiol. Biophys.*, 1986, **5**, 391–403.
160 W. E. Brownell, F. Qian and B. Anvari, *Biophys. J.*, 2010, **99**, 845–852.
161 W. Brownell, B. Farrell and R. Raphael, *BIOPHYSICS OF THE COCHLEA From Molecules to Models*, Proceedings of the International Symposium, Titisee, Germany, 2002.
162 W. Brownell, A. Spector, R. Raphael and A. Popel, *Annu. Rev. Biomed. Eng.*, 2001, **3**, 169–194.
163 K. D. Breneman, W. E. Brownell and R. D. Rabbitt, *PLoS One*, 2009, **4**, e5201.
164 M. Majdoub, P. Sharma and T. Cagin, *Phys. Rev. B: Condens. Matter Mater. Phys.*, 2008, **77**, 125424.
165 Y. Qi, J. Kim, T. D. Nguyen, B. Lisko, P. K. Purohit and M. C. McAlpine, *Nano Lett.*, 2011, **11**, 1331–1336.
166 M. Majdoub, P. Sharma and T. Çağin, *Phys. Rev. B: Condens. Matter Mater. Phys.*, 2008, **78**, 121407.

167 K. Wang and B. Wang, *Int. J. Eng. Sci.*, 2017, **116**, 88–103.
168 K. Wang and B. Wang, *Compos. Struct.*, 2016, **153**, 253–261.
169 J. K. Han, S. Y. C. Do Hyun Jeon, S. W. Kang, S. A. Yang, S. D. Bu, S. Myung, J. Lim, M. Choi, M. Lee and M. K. Lee, *Sci. Rep.*, 2016, **6**, 29562.
170 Q. Deng, M. Kammoun, A. Erturk and P. Sharma, *Int. J. Solids Struct.*, 2014, **51**, 3218–3225.
171 T. Rafael, B. Ghoncheh Kasiri and M. Fabio La, *J. Phys.: Condens. Matter*, 2016, **28**, 114005.
172 A. Morozovska, E. Eliseev and S. Kalinin, *J. Appl. Phys.*, 2012, **111**, 014114.
173 A. Morozovska, E. Eliseev, A. Tagantsev, S. Bravina, L.-Q. Chen and S. Kalinin, *Phys. Rev. B: Condens. Matter Mater. Phys.*, 2011, **83**, 195313.
174 P. Yu, S. Hu and S. Shen, *J. Appl. Phys.*, 2016, **120**, 065102.
175 M. Spassova, A. Petrov and J. Fendler, *J. Phys. Chem.*, 1995, **99**, 9485–9490.
176 K. Chu, B.-K. Jang, J. H. Sung, Y. A. Shin, E.-S. Lee, K. Song, J. H. Lee, C.-S. Woo, S. J. Kim, S.-Y. Choi, T. Y. Koo, Y.-H. Kim, S.-H. Oh, M.-H. Jo and C.-H. Yang, *Nat. Nanotechnol.*, 2015, **10**, 972–979.
177 S. V. Kalinin and A. N. Morozovska, *Nat. Nanotechnol.*, 2015, **10**, 916–917.
178 T. Ohta, S. Asakura, M. Yamaguchi, N. Kamiya, N. Gotgh and T. Otagawa, *Int. J. Hydrogen Energy*, 1976, **1**, 113–116.
179 T. Ohta, N. Kamiya, M. Yamaguchi, N. Gotoh, T. Otagawa and S. Asakura, *Int. J. Hydrogen Energy*, 1978, **3**, 203–208.
180 Y. Chen, M. Chen, N. Shen and R. J. Zeng, *Int. J. Hydrogen Energy*, 2016, **41**, 22760–22768.
181 J.-Y. Jung and J.-H. Lee, *SPIE Newsroom*, 2016, DOI: 10.1117/2.1201512.006219.
182 Z. Liu, X. Cao, B. Wang, M. Xia, S. Lin, Z. Guo, X. Zhang and S. Gao, *J. Power Sources*, 2017, **342**, 452–459.
183 V. Andrei, K. Bethke and K. Rademann, *Energy Environ. Sci.*, 2016, **9**, 1528–1532.
184 W. B. Chang, H. Fang, J. Liu, C. M. Evans, B. Russ, B. C. Popere, S. N. Patel, M. L. Chabinyc and R. A. Segalman, *ACS Macro Lett.*, 2016, **5**, 455–459.
185 A. Fujishima and K. Honda, *Nature*, 1972, **238**, 37–38.
186 T. Inoue, A. Fujishima, S. Konishi and K. Honda, *Nature*, 1979, **277**, 637–638.
187 R. Abe, *J. Photochem. Photobiol., C*, 2010, **11**, 179–209.
188 C. Acar and I. Dincer, *Int. J. Hydrogen Energy*, 2016, **41**, 7950–7959.
189 M. G. Walter, E. L. Warren, J. R. McKone, S. W. Boettcher, Q. Mi, E. A. Santori and N. S. Lewis, *Chem. Rev.*, 2010, **110**, 6446–6473.
190 K. Malik, S. Singh, S. Basu and A. Verma, *Wiley Interdiscip. Rev.: Energy Environ.*, 2017, **6**, 1–17.
191 X. Chang, T. Wang and J. Gong, *Energy Environ. Sci.*, 2016, **9**, 2177–2196.
192 P. Lianos, *J. Hazard. Mater.*, 2011, **185**, 575–590.
193 A. G. Gutierrez-Mata, S. Velazquez-Martínez, A. Álvarez-Gallegos, M. Ahmadi, J. A. Hernández-Pérez, F. Ghanbari and S. Silva-Martínez, *Int. J. Photoenergy*, 2017, **2017**, 1–27.
194 R. B. P. Marcelino, M. T. A. Queiroz, C. C. Amorim, M. M. D. Leão and F. F. Brites-Nóbrega, *Environ. Sci. Pollut. Res.*, 2015, **22**, 762–773.
195 W. Wu and Z. L. Wang, *Nat. Rev. Mater.*, 2016, **1**, 16031.
196 D. Lincot, *C. R. Phys.*, 2017, DOI: 10.1016/j.crhy.2017.09.003.
197 S. A. Bonke, M. Wiechen, D. R. MacFarlane and L. Spiccia, *Energy Environ. Sci.*, 2015, **8**, 2791–2796.
198 M. Gong, W. Zhou, M. J. Kenney, R. Kapusta, S. Cowley, Y. Wu, B. Lu, M.-C. Lin, D.-Y. Wang, J. Yang, B.-J. Hwang and H. Dai, *Angew. Chem., Int. Ed.*, 2015, **54**, 11989–11993.
199 L. Han, I. A. Digdaya, T. W. F. Buijs, F. F. Abdi, Z. Huang, R. Liu, B. Dam, M. Zeman, W. A. Smith and A. H. M. Smets, *J. Mater. Chem. A*, 2015, **3**, 4155–4162.
200 J. Jia, L. C. Seitz, J. D. Benck, Y. Huo, Y. Chen, J. W. D. Ng, T. Bilir, J. S. Harris and T. F. Jaramillo, *Nat. Commun.*, 2016, **7**, 13237.
201 J. Sun, D. K. Zhong and D. R. Gamelin, *Energy Environ. Sci.*, 2010, **3**, 1252–1261.
202 B. Zhang, Q. Daniel, M. Cheng, L. Fan and L. Sun, *Faraday Discuss.*, 2017, **198**, 169–179.
203 N. Gaillard and A. Deangelis, in *Solar to Chemical Energy Conversion: Theory and Application*, ed. M. Sugiyama, K. Fujii and S. Nakamura, Springer International Publishing, Cham, 2016, pp. 261–279.
204 S. Rau, S. Vierrath, J. Ohlmann, A. Fallisch, D. Lackner, F. Dimroth and T. Smolinka, *Energy Technol.*, 2014, **2**, 43–53.
205 D. Shapiro, J. Duffy, M. Kimble and M. Pien, *Solar Energy*, 2005, **79**, 544–550.
206 R. Li, *Chin. J. Catal.*, 2017, **38**, 5–12.
207 F. Yilmaz, M. T. Balta and R. Selbaş, *Renewable Sustainable Energy Rev.*, 2016, **56**, 171–178.
208 Y. Izumi, *Coord. Chem. Rev.*, 2013, **257**, 171–186.
209 M. Schreier, F. Héroguel, L. Steier, S. Ahmad, J. S. Luterbacher, M. T. Mayer, J. Luo and M. Grätzel, *Nat. Energy*, 2017, **2**, 17087.
210 Gurudayal, J. Bullock, D. F. Sranko, C. M. Towle, Y. Lum, M. Hettick, M. C. Scott, A. Javey and J. Ager, *Energy Environ. Sci.*, 2017, **10**, 2222–2230.
211 H. S. Jeon, J. H. Koh, S. J. Park, M. S. Jee, D.-H. Ko, Y. J. Hwang and B. K. Min, *J. Mater. Chem. A*, 2015, **3**, 5835–5842.
212 M. Schreier, L. Curvat, F. Giordano, L. Steier, A. Abate, S. M. Zakeeruddin, J. Luo, M. T. Mayer and M. Grätzel, *Nat. Commun.*, 2015, **6**, 7326.
213 M. R. Singh, E. L. Clark and A. T. Bell, *Proc. Natl. Acad. Sci. U. S. A.*, 2015, **112**, E6111–E6118.
214 F. Hussin, F. Abnisa, G. Issabayeva and M. K. Aroua, *J. Cleaner Prod.*, 2017, **147**, 206–216.
215 N. Pichel, M. Vivar and M. Fuentes, *Appl. Energy*, 2016, **171**, 103–112.
216 B. S. Richards and A. I. Schäfer, *Renewable Energy*, 2003, **28**, 2013–2022.
217 B. S. Richards, J. Shen and A. I. Schäfer, *Energy Technol.*, 2017, **5**, 1112–1123.
218 A. K. Pandey, V. V. Tyagi, J. A. L. Selvaraj, N. A. Rahim and S. K. Tyagi, *Renewable Sustainable Energy Rev.*, 2016, **53**, 859–884.

219 Y. Wang, Y. Jin, Q. Huang, L. Zhu, M. Vivar, L. Qin, Y. Sun, Y. Cui and L. Cui, *Energy*, 2016, **106**, 757–764.
220 O'Callaghan H. L. and B. N. & Norton, presented in part at the Civil Engineering Research in Ireland Conference, (CERI2016) NUI Galway from 29–30 August, 2016.
221 R. Long, B. Li, Z. Liu and W. Liu, *Chem. Eng. J.*, 2016, **284**, 325–332.
222 Z. Wang, *Nature*, 2017, **542**, 159–160.
223 S. Priya, H.-C. Song, Y. Zhou, R. Varghese, A. Chopra, S.-G. Kim, I. Kanno, L. Wu, S. Ha Dong, J. Ryu and G. Polcawich Ronald, *Energy Harv. Syst.*, 2017, **4**, 3.
224 D. Choi, Y.-H. Tsao, C.-M. Chiu, D. Yoo, Z.-H. Lin and D. S. Kim, *Nano Energy*, 2017, **38**, 419–427.
225 K. Asadi and M. A. van der Veen, *Eur. J. Inorg. Chem.*, 2016, 4332–4344.
226 X. Crispin, M. Berggren and H. Wang, *European Pat.*, EP2662908 A3, 2014.
227 L. Wang, Y. Liu, Z. Zhang, B. Wang, J. Qiu, D. Hui and S. Wang, *Composites, Part B*, 2017, **122**, 145–155.
228 Z. Ahmad, K. S. Karimov, F. Touati, M. S. Ajmal, T. Ali, S. H. Kayani, K. Kabutov, R. A. Shakoor and N. J. Al-Thani, *J. Electroanal. Chem.*, 2016, **775**, 267–272.
229 S. Matsushita, A. Tsuruoka, E. Kobayashi, T. Isobe and A. Nakajima, *Mater. Horiz.*, 2017, **4**, 649–656.
230 L. Zhang, T. Kim, N. Li, T. J. Kang, J. Chen, J. M. Pringle, M. Zhang, A. H. Kazim, S. Fang, C. Haines, D. Al-Masri, B. A. Cola, J. M. Razal, J. Di, S. Beirne, D. R. MacFarlane, A. Gonzalez-Martin, S. Mathew, Y. H. Kim, G. Wallace and R. H. Baughman, *Adv. Mater.*, 2017, **29**, 1605652.
231 P. F. Salazar, S. Kumar and B. A. Cola, *J. Appl. Electrochem.*, 2014, **44**, 325–336.
232 H. Im, T. Kim, H. Song, J. Choi, J. S. Park, R. Ovalle-Robles, H. D. Yang, K. D. Kihm, R. H. Baughman, H. H. Lee, T. J. Kang and Y. H. Kim, *Nat. Commun.*, 2016, **7**, 10600.
233 M. F. Dupont, D. R. MacFarlane and J. M. Pringle, *Chem. Commun.*, 2017, **53**, 6288–6302.
234 R. Hu, B. A. Cola, N. Haram, J. N. Barisci, S. Lee, S. Stoughton, G. Wallace, C. Too, M. Thomas, A. Gestos, M. E. d. Cruz, J. P. Ferraris, A. A. Zakhidov and R. H. Baughman, *Nano Lett.*, 2010, **10**, 838–846.
235 S. W. Lee, Y. Yang, H.-W. Lee, H. Ghasemi, D. Kraemer, G. Chen and Y. Cui, *Nat. Commun.*, 2014, **5**, 3942.
236 C. Gao, S. W. Lee and Y. Yang, *ACS Energy Lett.*, 2017, 2326–2334, DOI: 10.1021/acsenergylett.7b00568.
237 C. F. Gerald, D. Mitchell and R. T. Foley, *J. Electrochem. Soc.*, 1973, **120**, 236–241.
238 R. L. Curl, *Int. J. Hydrogen Energy*, 1979, **4**, 13–20.
239 W. Wu, C. Zhang and S. Hou, *J. Mater. Sci.*, 2017, **52**, 10649–10660.
240 L. Lappeenranta, University of Technology, Protein produced with electricity to alleviate world hunger, https://www.sciencedaily.com/releases/2017/07/170719090025.htm, July 19, 2017.